Table 2.1: Leptonic decay constant f_H (in MeV)

f_H	Present	Data	Refrences
f_D	206.08	202.2(2.2)(2.6)	LQCD [?]
		210 ± 11	QCDSR [?]
		211.9(1.1)	PDG [12]
f_{Ds}	257.70	258.7 (1.1) (2.9)	LQCD [?]
		259 ± 10	QCDSR [?]
		249.0(1.2)	PDG [12]
f_{Ds}/f_D	1.25	1.173(3)	PDG [12]
f_K	156.96	155.37(34)	LQCD [?]
		157.9 ± 1.5	LQCD [?]
		155.6(0.4)	PDG [12]
f_π	130.30	130.39 (20)	LQCD [?]
		132.3 ± 1.6	LQCD [?]
		130.2(1.7)	PDG [12]
f_K/f_π	1.20	1.1928(26)	PDG [12]
f_{D^*}	244.27	$278. \pm 13 \pm 10$	LQCD [?]
		263 ± 21	QCDSR [?]
$f_{D_s^*}$	272.08	311 ± 9	LQCD [?]
		308 ± 21	QCDSR [?]
f_{K^*}	226.81	222 ± 8	QCDSR [?]
f_ρ	218.28	$208.5 \pm 55 \pm 0.9$	LQCD [?]
f_ϕ	226.56	238 ± 3	LQCD [?]
		215 ± 5	QCDSR [?]
f_ω	198.38	194.6 ± 3.24	LFQM [8]

Table 2.2: CCQM model parameters: quark masses, meson size parameters and infrared cut-off parameter (all in GeV)

Λ_B	Λ_{B_s}	Λ_π	$\Lambda_{\bar{K}^0}$	Λ_ρ	$\Lambda_{\bar{K}^{*}(892)^0}$	Λ_{Ds}
1.963 ± 0.038	2.05 ± 0.036	0.871 ± 0.002	1.014 ± 0.008	0.610 ± 0.012	0.81 ± 0.024	1.75 ± 0.035
$m_{u/d}$	m_s	m_c	m_b	λ	Λ_ω	Λ^*_{Ds}
0.241	0.428	1.67	5.05	0.181	0.488 ± 0.019	1.56 ± 0.014

Chapter 3

Weak Decays Of Meson

3.1 Introduction

When looking into the physics of weak transition, semileptonic decays are one of the crucial tools. Both within and outside of the SM, they have profound phenomenological ramification for the particle physics. When measuring the elements of the Cabibbo-Kobayashi-Maskawa (CKM) matrix, weak decays involving quark mixing serve a crucial probe. In addition to various types of weak decays, the coupling of heavy quark dynamics V_{cb} is supplied via the tree level transition $b \to c\ell\nu_\ell$. During the course of the previous few years, numerous novel findings of $B \to D^{(*)}\ell\nu_\ell$ decays have been reported by experimental facilities available worldwide. The fact that many of these observations contradict the expectations of SM raises the prospect of New Physics (NP) being involved in the processes that are being studied here. Other data available from the lattice can be used to analyse these channels. These abnormalities are reported in the recent review article [138] and the references therein. The sole distinction between $B \to D^{(*)}\ell\nu_\ell$ and $B_s \to D_s^{(*)}\ell\nu_\ell$ decay channel is the difference between the spectator quarks. As a result, it is adequate to anticipate that these channels will also exhibit comparable oddities. Additionally, it can be used as an appealing prospect for the estimation of V_{cb} as well as the investigation for NP that goes beyond the usual model. For the very first time, the LHCb collaboration has successfully measured the value of V_{cb} by using transition form factors and decay rates

of relevant channels [139]. Additionally, this is for the first time that the absolute branching fractions have been determined by them, and their findings are [139].

$$\begin{aligned}\mathcal{B}(B_s^0 \to D_s^- \mu^+ \nu_\mu)_{LHCb} &= (2.49 \pm 0.12(stat) \pm 0.14(syst) \pm 0.16(ext)) \times 10^{-2} \\ \mathcal{B}(B_s^0 \to D_s^{*-} \mu^+ \nu_\mu)_{LHCb} &= (5.38 \pm 0.25(stat) \pm 0.46(syst) \pm 0.30(ext)) \times 10^{-2}\end{aligned} \tag{3.1}$$

and the ratio of both the channels is also calculated as

$$\frac{\mathcal{B}(B_s^0 \to D_s^- \mu^+ \nu_\mu)_{LHCb}}{\mathcal{B}(B_s^0 \to D_s^{*-} \mu^+ \nu_\mu)_{LHCb}} = 0.464 \pm 0.013(stat) \pm 0.043(syst) \tag{3.2}$$

Precise data from Lattice calculations are also available for the determination of V_{cb}, due to the fact that higher valance s quark mass in B_s transition makes the computation of form factor somewhat less expensive. Very recently the results of transition form factor, branching fraction and ratio of branching fraction have been provided by HPQCD collaboration [140,141] that matches well with the results provided by LHCb experiments. The ratio of the branching fraction is given as

$$\frac{\mathcal{B}(B_s^0 \to D_s^- \mu^+ \nu_\mu)_{HPQCD}}{\mathcal{B}(B_s^0 \to D_s^{*-} \mu^+ \nu_\mu)_{HPQCD}} = 0.429(43)_{latt}(4)_{EM} \tag{3.3}$$

Further, $R(D_s)$ and $R(D_s^*)$ ratio has also been provided by them which reads as

$$\begin{aligned}R(D_s)_{HPQCD} &= \frac{\mathcal{B}(B_s \to D_s \tau \nu_\tau)}{\mathcal{B}(B_s \to D_s \ell \nu_\ell)} = 0.2993(46) \\ R(D_s^*)_{HPQCD} &= \frac{\mathcal{B}(B_s \to D_s^* \tau \nu_\tau)}{\mathcal{B}(B_s \to D_s^* \ell \nu_\ell)} = 0.2442(79)_{latt}(35)_{EM}\end{aligned} \tag{3.4}$$

here the ratio is between tau mode to electron mode or muon mode. Results of transition form factors and branching fractions have been computed using many other theoretical approaches namely by Perturbative QCD factorization approach [142], Light Cone QCD Sum Rule [143–145] and using three point sum rule [146]. Some results are also available using Light Front Quark Model [8,147,148], RQM [149] and Constituent Quark Model [150].

We have calculated transition form factors in the entire physical range of momentum

transfer, on top of that branching fraction and ratio of branching fractions are also calculated. Further, to probe the lepton flavor universality, we have determined the ratio of branching fraction of electron or muon with tau mode for both D_s and D_s^* mesons. In addition, we have also provided the results for some physical observables like forward-backward asymmetry and longitudinal polarization for leptons in $B_s \to D_s \ell \nu_\ell$ and $B_s \to D_s^* \ell \nu_\ell$ transitions. The results for these physical observables are still awaited from experiments, which makes it a detailed study by itself.

In 2022, Belle II detector announced the result for partial branching fraction for $B^0 \to \pi^- e^+ \nu_e$ and $B^0 \to \pi^- \mu^+ \nu_\mu$ decays as a function of q^2 and total branching fraction for $B^0 \to \pi^- \ell^+ \nu_\ell$ is also measured [151]. Following this, Heavy Flavor Averaging Group (HFLAV) in 2023 reported branching fraction and q^2 spectrum results for $b \to \pi \ell \nu_\ell$ decays [152]. Previously, branching fraction, q^2 distribution and shape of the form factor for different channels ($B \to (\pi/\rho/\eta/\eta^{'})\ell\nu_\ell$) corresponding to $b \to u$ transition have been reported by CLEO [153–155] and BABAR [156–159] collaborations. All the above experimental collaborations have also reported the value of V_{ub} which requires accurate measurement of transition form factors. Semileptonic form factor for $B^0 \to \pi^+ \ell \nu_\ell$ decay have been calculated using $2+1$ flavor lattice QCD in high $q^2 (\geq 16 GeV^2/c^2)$ region which also demands for the determination of branching fraction in the same q^2 region [52]. Authors of [53] have also calculated B meson semileptonic form factors using unquenched lattice QCD for $B \to \pi \ell \nu_\ell$ transition. $b \to u$ transition form factors at small and intermediate values of q^2 have been calculated for $B \to \pi/K/\eta$ using QCD light cone sum rule with pion distribution amplitudes [160–162], where the q^2_{max} varies between 12 to 16 GeV^2.

Transition form factor and decay rates for exclusive rare decay $B_s \to (K, \eta, \eta^{'})\ell^+\ell^-$ is calculated in Light Front Quark Model (LQFM) [46, 163]. Form factors, differential decay rates, branching fraction and ratio of differential branching fraction for $B_s \to K$ have been calculated in LQCD [11, 164–166], RQM [4], Light Cone Quark Model(LCQM) [167], Light Cone Sum Rule (LCSR) [160], pQCD approach [2, 168, 169]. Recently, the first experimental result was produced by LHCb for the branching fraction of $B_s \to K$ decay [170]. All these results provide necessary stimulations to study $b \to u$ decay in more detail.

3.2 Methodology

The invariant formulation of matrix element neglecting correction from QED can be given by

$$\mathcal{M}(M_1 \to M_2^* \ell^+ \nu_\ell) = \frac{G_F}{\sqrt{2}} V_{CKM} \langle M_2^* | \bar{q}_2 O^\mu q_1 | M_1 \rangle [\ell^+ O_\mu \nu_\ell] \tag{3.5}$$

the matrix elements in CCQM is shown in the Fig. 3.1 and defined in terms of form factors as

$$\begin{aligned}
\langle M_2(p_2)|\bar{q}_2 O^\mu q_1|M_1(p_1)\rangle &= N_c g_{M_1} g_{M_2} \\
&\times \int \frac{d^4k}{(2\pi)^4 i} \Phi_{M_1}(-(k+w_{13}p_1)^2) \Phi_{M_2}(-(k+w_{23}P_2)^2) \\
&\times \mathrm{tr}[O^\mu S_1(k+p_1)\gamma^5 S_3(k) S_2(k+p_2)] \\
&= F_+(q^2)P^\mu + F_-(q^2)q^\mu,
\end{aligned} \tag{3.6}$$

$$\begin{aligned}
\langle M_2(p_2)|\bar{q}_2 \sigma^{\mu\nu}(1-\gamma^5) q_1|M_1(p_1)\rangle &= N_c g_{M_1} g_{M_2} \\
&\times \int \frac{d^4k}{(2\pi)^4 i} \tilde{\phi}_{M_1}(-(k+w_{13}p_1)^2) \tilde{\phi}_{M_2}(-(k+w_{23}p_2)^2) \\
&\times \mathrm{tr}[\sigma^{\mu\nu}(1-\gamma^5) S_1(k+p_1)\gamma^5 S_3(k)\gamma^5 S_2(k+p_2)] \\
&= \frac{iF_T(q^2)}{m_1+m_2}(P^\mu q^\nu - P^\nu q^\mu + i\varepsilon^{\mu\nu Pq}).
\end{aligned} \tag{3.7}$$

$$\begin{aligned}
\langle M_2^*(p_2,\epsilon_\nu)|\bar{q}_2 O^\mu q_1|M_1(p_1)\rangle &= N_c g_{M_1} g_{M_2^*} \\
&\int \frac{d^4k}{(2\pi)^4 i} \Phi_{M_1}(-(k+w_{13}p_1)^2) \Phi^*_{M_2}(-(k+w_{23}P_2)^2) \\
&\times \mathrm{tr}[O^\mu S_1(k+p_1)\gamma^5 S_3(k) \not{\epsilon}_2^\dagger S_2(k+p_2)] \\
&= \frac{\epsilon_\nu^\dagger}{m_{M_1}+m_{M_2}}[-g^{\mu\nu} P\cdot q A_0(q^2) + P^\mu P^\nu A_+(q^2) \\
&+ q^\mu P^\nu A_-(q^2) + i\varepsilon^{\mu\nu\alpha\beta} P_\alpha q_\beta V(q^2)]
\end{aligned} \tag{3.8}$$

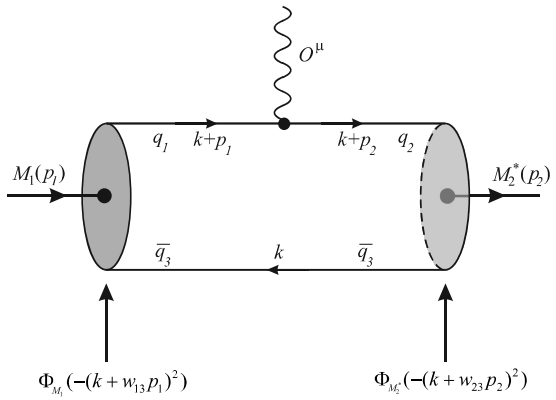

Figure 3.1: Quark model diagram for semi-leptonic decay of meson

$$\begin{aligned}\langle M_2^*(p_2,\epsilon)|\bar{q}_2\sigma^{\mu\nu}q_\nu(1+\gamma^5)q_1|M_1(p_1)\rangle &= N_c g_{M_1} g_{M_2} \\ &\times \int \frac{d^4k}{(2\pi)^4 i}\tilde{\phi}_{M_1}(-(k+w_{13}p_1)^2)\tilde{\phi}_{M_2^*}(-(k+w_{23}p_2)^2) \\ &\times \mathrm{tr}[\sigma^{\mu\nu}q_\nu(1+\gamma^5)S_1(k+p_1)\gamma^5 S_3(k)\ \not{\epsilon}_\nu^\dagger S_2(k+p_2)] \\ &= \epsilon_\nu^\dagger(-(g^{\mu\nu}-q^\mu q^\nu/q^2)P\cdot q a_0(q^2) \\ &+ (P^\mu P^\nu - q^\mu P^\nu P\cdot q/q^2)a_+(q^2) + i\varepsilon^{\mu\nu\alpha\beta}P_\alpha q_\beta g(q^2))\end{aligned} \tag{3.9}$$

Double-pole representation of form factor of Eq. (3.6) − (3.9) is given as

$$F(q^2) = \frac{F(0)}{1 - a(\frac{q^2}{m_{M_1}^2}) + b(\frac{q^2}{m_{M_1}^2})^2} \tag{3.10}$$

where weak Dirac matrix is given by $O^\mu = \gamma_\mu(1-\gamma_5)$ and G_F is the Fermi's coupling constant. ϵ_v is the polarization vector such that $\epsilon_v \cdot p_2 = 0$. $P = p_1 + p_2$ and $q = p_1 - p_2$. $p_1^2 = m_{M_1}^2$ and $p_2^2 = m_{M_2}^2$ satisfies the on-shell condition. These processes involves three flavors of quarks, q_1, q_2, and q_3, where q_3 is spectator quark and hence notion with two subscripts $w_{ij} = m_i/(m_i + m_j)$, where $i, j = 1, 2, 3$ such that $w_{ij} + w_{ji} = 1$ will suffice. Using Eq. (3.6) − (3.8) form factor and branching fraction have been calculated for both $B_s \to D_s^*$ and $B_s \to K^*$ semileptonic decays by model independent approach. We have related our form factors calculated in Eq. (3.6) − (3.8) with Bauer-Stech-Wirbel (BSW) form factors [171] so that we can compare them effectively with other theoretical approaches. Differential decay rates for $q_1 \to q_2$ transition is described

using helicity amplitudes which reads as

$$\frac{d\Gamma(M_1 \to M_2^{(*)} \ell^+ \nu_\ell)}{dq^2} = \frac{G_F^2 |V_{CKM}|^2 |\boldsymbol{p}_2| q^2 v^2}{12(2\pi)^3 m_{M_1}^2} \times \Big[(1+\delta_\ell)|H_n|^2 + 3\delta_\ell |H_t|^2 \Big] \tag{3.11}$$

Where, $|H_n|^2 = |H_+|^2 + |H_-|^2 + |H_0|^2$. The momentum for the daughter meson is given by $|\boldsymbol{p}_2| = \lambda^{1/2}(m_{M_1}^2, m_{M_2}^2, q^2)/2m_{M_1}$, where λ is the *Källen* function. Here $v = 1 - m_\ell^2/q^2$ and helicity flip factor is given by $\delta_\ell = m_\ell^2/2q^2$. In above equation, the H_t, H_0 and $H_\pm$ are bilinear combinations of helicity amplitudes. For $M_1 \to M_2\ \ell^+\nu_\ell$ they are defined as

$$\begin{aligned} H_t &= \frac{1}{\sqrt{q^2}}(P_q F_+ + q^2 F_-), \\ H_\pm &= 0, \\ H_0 &= \frac{2m_{M_1}|\boldsymbol{p}_2|}{\sqrt{q^2}} F_+ \end{aligned} \tag{3.12}$$

for $M_1 \to M_2^*\ \ell^+\nu_\ell$ they are defined as

$$\begin{aligned} H_t &= \frac{1}{m_{M_1}+m_{M_2}} \frac{m_{M_1}|\boldsymbol{p}_2|}{m_{M_2}\sqrt{q^2}}((m_{M_1}^2 - m_{M_2}^2)(A_+ - A_-) + q^2 A_-), \\ H_\pm &= \frac{1}{m_{M_1}+m_{M_2}}(-(m_{M_1}^2 - m_{M_2}^2)A_0 \pm 2m_{M_2}|\boldsymbol{p}_2|V), \\ H_0 &= \frac{1}{m_{M_1}+m_{M_2}} \frac{1}{2m_{M_2}\sqrt{q^2}}(-(m_{M_1}^2 - m_{M_1}^2)(m_{M_1}^2 - m_{M_2}^2 - q^2)A_0 + 4m_{M_1}^2|\boldsymbol{p}_2|^2 A_+). \end{aligned} \tag{3.13}$$

In the equations above, M_1 and M_2 represent the parent and daughter mesons and m_{M_1} and m_{M_2} represent the mass of parent and daughter respectively. The size parameters for mesons listed in Tab. 2.2 along with compositeness condition are used to compute coupling strength of meson for all channels considered. Model independent parameters such as meson masses, lifetime, CKM matrix element and Fermi coupling constant are taken from Particle Data Group (PDG) [172]. Application of the mentioned framework will be discussed in Sec. 3.4 and 3.5.

3.3 Estimation of Uncertainty and its Propagation

Minimum deviation in the computation of decay constant is guaranteed by the parametrization onto the functional given by [173, 174],

$$\chi^2 = \sum_i \frac{(y_i^{experiment} - y_i^{thoery})^2}{\sigma_i^2}$$

where σ_i are the experimental standard deviation. The absolute uncertainty in size parameter was determined individually by changing the respective parameter and keeping other parameters unchanged till the result matches with experimental or lattice data. The uncertainty obtained in this manner is found to be within 5% for all flavoured mesons. Once the absolute uncertainties in size parameters are determined, they are transported to the form factor in the whole q^2 range where uncertainties in the form factor are found to be less than 10% at the maximum recoil. In this study the number of size parameters are 9 and number of decay constants used to fit the size parameters are 12 so D.o.f are 3. The propagation of error in branching fraction is computed in the most general way by writing the differential decay rate Eq. (3.11) in terms of the form factor as

$$\frac{d\mathcal{B}}{dq^2} = N(aF_+^2(q^2) + bF_-^2(q^2) + cF_+(q^2)F_-(q^2)) \tag{3.14}$$

Here a, b and c denotes the coefficients of form factors of helicity structure function defined in the Eq. (3.12). Other constants like CKM matrix element, Fermi coupling constant, meson mass etc are collectively represented by N. Now the total uncertainty in differential branching fraction is computed by estimating the total change in $d\mathcal{B}$ with respect to F_+ and F_- as

$$d(\Delta\mathcal{B}) = dq^2 N \sqrt{\left(\frac{\partial(d\mathcal{B})}{\partial F_+}\Delta F_+\right)^2 + \left(\frac{\partial(d\mathcal{B})}{\partial F_-}\Delta F_-\right)^2} \tag{3.15}$$

Here ΔF_+ and ΔF_- are calculated by myltiplying F_+ and F_- by their respective relative error which is shown as

$$(\Delta F_i)^2 = (F_i \times \epsilon_i)^2$$

Here ϵ is the relative error for respective form factor. Finally the Eq. (3.15) is integrated to obtain the total uncertainty in branching fraction. It is important to note that the uncertainty in form factor is also calculated using the same approach.

3.4 $b \to (c, u)\ell\nu_\ell$ Transition

3.4.1 Result and Discussion for $B_s \to K^{(*)-}$ Channels

Transition form factors for semileptonic $B_s \to K^{(*)-}$ channels are calculated using the methodology described in Sec. 3.2. Form factors are also represented in double pole parametrization Eq. (3.10). Form Factor at origin and associated double pole parameters are listed in Tab. 3.1. For $B_s \to K^{(*)-}$ decay, matrix elements are calculated using Eq. (3.6) − (3.9), where M_1 and M_2 represent the B_s and K mesons respectively. Double pole representation of the form factor of Eq. (3.6) − (3.9) can be given by Eq. (3.10) and the result is tabulated in Tab. 3.1 and plotted in Fig. 3.2.

Table 3.1: Form factors and double pole parameters for $B_s \to K^{(*)-}$ transitions

F	$F(0)$	a	b	F	$F(0)$	a	b
$F_+^{B_s\to K}$	0.247 ± 0.016	1.441	0.465	$F_-^{B_s\to K}$	-0.205 ± 0.013	1.474	0.494
$F_T^{B_s^0\to \bar{K}^0}$	0.256 ± 0.016	1.429	0.451	$A_+^{B_s\to K^*}$	0.210 ± 0.015	1.463	0.435
$A_-^{B_s\to K^*}$	-0.228 ± 0.016	1.539	0.504	$A_0^{B_s\to K^*}$	0.300 ± 0.021	0.654	-0.262
$V^{B_s\to K^*}$	0.244 ± 0.018	1.584	0.545	$g^{B_s^0\to \bar{K}^*(892)^0}$	0.210 ± 0.015	1.597	0.559

For $B_s \to K^{(*)-}$ channel, transition form factors are calculated in entire physical range of momentum transfer. Comparison of calculated form factors with other theoretical approaches are given in Tab. 3.2. Differential decay rates are also computed and plotted in Fig. 3.3. Next, we have computed semileptonic branching fraction using the Eq. (3.11) and results are compared with other theoretical approaches as well as with the available experimental data and tabulted in Tab. 3.4. It is seen that our

Table 3.2: Form factors for $B_s \to K$ transitions at maximum recoil

Theory	$B_s \to K$	
	$f_{+,0}(0)$	$f_T(0)$
Present	0.247 ± 0.015	0.256 ± 0.016
LCSR [47]	0.364	0.363
LCSR [7]	0.296 ± 0.018	$0.288^{+0.018}_{-0.017}$
LCSR [48]	0.336 ± 0.023	0.320 ± 0.019
LCSR [49]	- - -	- - -
SUSY [5]	- - -	- - -
pQCD [2]	$0.26^{+0.04}_{-0.03} \pm 0.03 \pm 0.02$	$0.28 \pm 0.04 \pm 0.03 \pm 0.02$
pQCD [14]	0.22	0.22
SCET [167]	0.297	0.325
RQM [3, 4]	0.284	0.236
CQM [6]	0.31	0.31
LFQM [8]	0.23	- - -

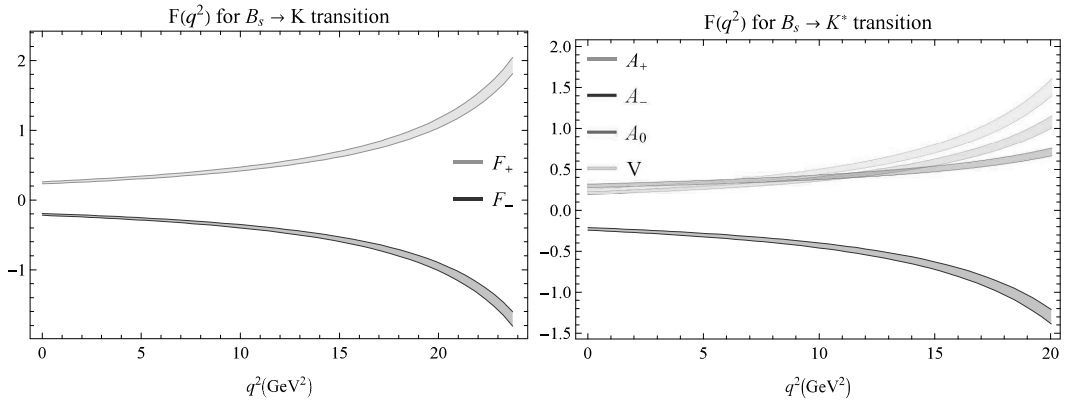

Figure 3.2: Form factor for $B_s \to K^{(*)-}$ transitions

Table 3.3: Form factors for $B_s \to K^*(892)$ transition at maximum recoil

	$V(0)$	$A_0(0)$	$A_1(0)$	$A_2(0)$	$T_{1,2}(0)$	$T_3(0)$
Present	0.244 ± 0.018	0.225 ± 0.090	0.214 ± 0.015	0.210 ± 0.015	0.210 ± 0.015	0.156 ± 0.011
LCSR [7]	0.285 ± 0.013	- - -	$0.227^{+0.010}_{-0.012}$	$0.183^{+0.008}_{-0.010}$	0.251 ± 0.012	0.169 ± 0.008
LCSR [9]	0.31	0.36	0.23	0.18	0.26	0.14
LCSR [175]	0.296 ± 0.030	0.314 ± 0.048	0.230 ± 0.025	0.229 ± 0.035	0.239 ± 0.024	0.597 ± 0.076
pQCD [169]	$0.20^{+0.04+0.03}_{-0.04-0.02}$	$0.24^{+0.05+0.04}_{-0.04-0.02}$	$0.15^{+0.03+0.02}_{-0.03-0.01}$	$0.11^{+0.02+0.01}_{-0.02-0.01}$	$0.18^{+0.04+0.02}_{-0.03-0.0}$	$0.16^{+0.03+0.02}_{-0.03-0.02}$
pQCD [14]	0.24	0.21	0.19	0.19	0.21	0.16
SCET [167]	0.323	0.279	0.228	0.204	0.271	0.165
RQM [4]	0.291	0.289	0.287	0.286	0.238	0.122
CQM [6]	0.38	0.37	0.29	0.26	0.32	0.23
LFQM [10]	$0.28^{+0.02+0.07}_{-0.02-0.06}$	$0.22^{+0.01+0.06}_{-0.01-0.05}$	$0.20^{+0.01+0.05}_{-0.01-0.05}$	$0.19^{+0.01+0.05}_{-0.01-0.04}$	- - -	- - -

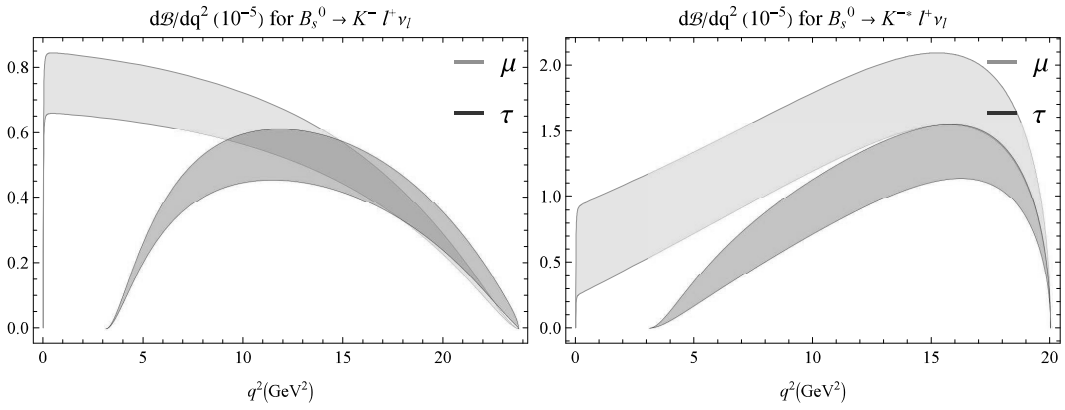

Figure 3.3: Differential decay rates for $B_s \to K^{(*)-}$ transitions

Table 3.4: Branching fraction for $B_s \to K^{(*)-}$ transitions (in the unit of 10^{-4})

Channel	Present	RQM [4]	LFQM [147]	LCSR [7]	LHCb [170]
$B_s \to Ke^+\nu_e$	1.24 ± 0.15	1.64 ± 0.17	1.0 ± 0.22	1.47 ± 0.15	- - -
$B_s \to K\mu^+\nu_\mu$	1.24 ± 0.15	- - -	- - -	- - -	$1.06^{\pm 0.05(stat)}_{\pm 0.08(syst)}$
$B_s \to K\tau^+\nu_\tau$	0.76 ± 0.12	0.96 ± 0.10	0.68 ± 0.15	1.02 ± 0.11	- - -
$B_s \to K^*e^+\nu_e$	2.64 ± 0.55	3.47 ± 0.35	3.3 ± 0.73	2.91 ± 0.26	- - -
$B_s \to K^*\mu^+\nu_\mu$	2.63 ± 0.55	- - -	- - -	- - -	- - -
$B_s \to K^*\tau^+\nu_\tau$	1.47 ± 0.27	1.67 ± 0.17	1.72 ± 0.38	1.58 ± 0.13	- - -

results for $B_s \to K^{(*)-}$ channels are in very good agreement with the experimental data given by LHCb [170] and also fall within the range given by LFQM [147] and LCSR [7] results. However, the results slightly deviates from the range given by RQM [4] approach. Computation of other physical observables like forward-backward asymmetry and longitudinal polarization will be discussed in next chapter for $B_s \to K^{(*)-}$ semileptonic decays.

3.4.2 Result and Discussion for $B_s \to D_s^{(*)-}$ Channels

Using the framework described in Sec. 3.2, we have obtained the results for the form factors, differential branching fraction and branching fraction for $B_s \to D_s^{(*)-}$ channels. For $B_s \to D_s^{(*)-}$ channels, the matrix elements in terms of form factors are given by Eq. (3.6) − (3.8). Propagation of the uncertainty in the calculation of form factor for semileptonic $B_s^0 \to D_s^{(*)-}$ channel is given in Fig. 3.4. Form factors with associated double-pole parameters for $B_s^0 \to D_s^{(*)-}$ channels are calculated and given in Tab. 3.5. Comparison of the calculated form factor at maximum recoil with other theoretical approaches are given in Tab. 3.6.

The transition form factor has been computed in the entire q^2 range using model parameters within the framework of CCQM. Calculated form factors have been compared with other theoretical approaches like relativistic quark model (RQM), perturbative

Table 3.5: Form factors and double pole parameters for $B_s \to D_s^{(*)-}$ transitions

F	$F(0)$	a	b	F	$F(0)$	a	b
$F_+^{B_s\to D_s}$	0.770±0.066	0.837	0.077	$F_-^{B_s\to D_s}$	-0.355±0.029	0.855	0.083
$A_+^{B_s\to D_s^*}$	0.630±0.025	0.972	0.092	$A_-^{B_s\to D_s^*}$	-0.756±0.031	1.001	0.116
$A_0^{B_s\to D_s^*}$	1.564±0.065	0.442	-0.178	$V^{B_s\to D_s^*}$	0.743±0.030	1.010	0.118

Table 3.6: Comparison of the form factors at maximum recoil $F(0)$ with other theoretical approaches

	$F_+(0)$	$V(0)$	$A_0(0)$	$A_1(0)$	$A_2(0)$
Present	0.770±0.066	0.743±0.030	0.719±0.070	0.681±0.065	0.630±0.025
RQM [149]	0.74±0.02	0.95±0.02	0.67±0.01	0.70±0.01	0.75±0.02
PQCD [142]	0.52±0.10	0.64±0.12	0.48±0.09	0.50±0.09	0.53±0.11
QCDSR [146]	0.7±0.1	0.63±0.05	0.52±0.06	0.62±0.1	0.75±0.07
LFQM [148]	- - -	$0.74^{+0.05}_{-0.05}$	$0.63^{+0.04}_{-0.04}$	$0.61^{+0.04}_{-0.04}$	$0.59^{+0.04}_{-0.04}$

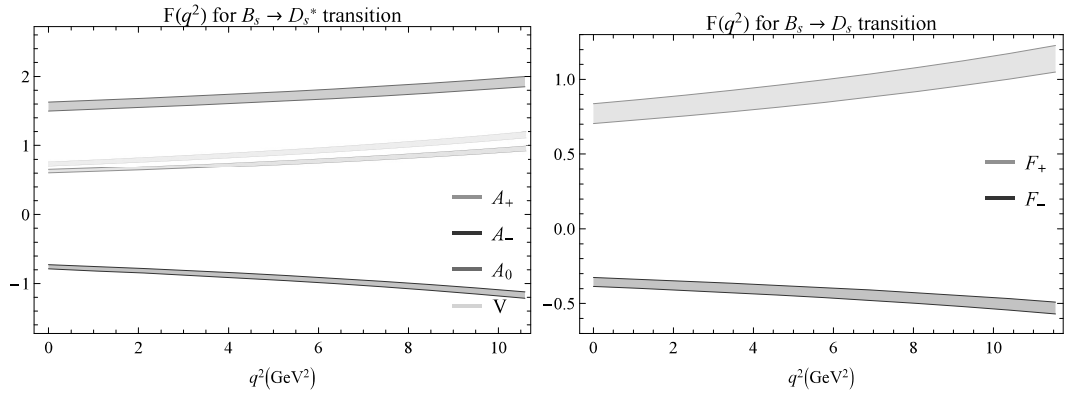

Figure 3.4: Form factor for $B_s \to D_s^{(*)-}$ transitions

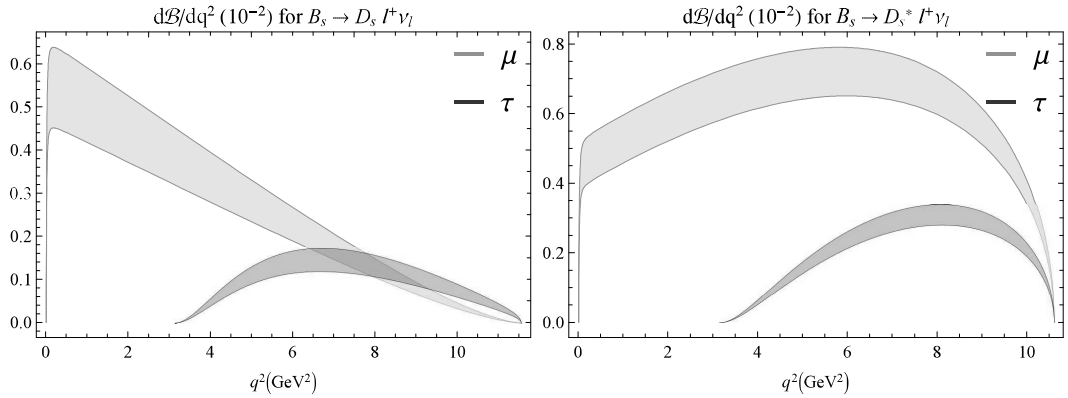

Figure 3.5: Differential decay rates for $B_s \to D_s^{(*)-}$ transitions

QCD (pQCD), light front quark model (LFQM) and QCD sum rules (QCDSR). Results show good match with RQM [149] other than $V(0)$, where as the results show very good agreement with LFQM [148] approach. Results deviate slightly more in comparison with pQCD [142]. Now employing the calculated transition form factors, differential decay rates given by Eq. (3.11) for semileptonic decay are computed. Normalized differential distribution for $B_s \to D_s^{(*)}$ channel has been plotted for muon and tau mode in Fig. 3.6. It is important to note here that the normalization is achieved using the total decay rate for muon mode. The spread in the plot of Fig. 3.5 point towards the propagated uncertainty arises solely from the uncertainties in calculated form factors. Normalized differential decay rates have been measured recently by LHCb [1] collaboration and later on by HPQCD [141] collaboration in terms of hadronic recoil parameter w for $B_s \to D_s^{(*)}\mu^+\nu_\mu$ channel. HPQCD collaboration has also provided the result for branching fraction for the same channel [141]. To present proper comparison with LHCb and lattice simulation, we have also computed

our result in terms of w, which is achieved by transforming the momentum transfer squared q^2 in terms of w using the relation [141]

$$w = \frac{m_{Bs}^2 + m_{Ds^*}^2 - q^2}{2m_{Bs}m_{Ds^*}} \tag{3.16}$$

Normalized differential decay rates in terms of recoil parameters have been plotted in Fig. 3.6 along with the recent results from LHCb data [139] and it is evident that our results are in very good agreement with LHCb data. Comparison of normalized decay rates in terms of small recoil parameter bins with lattice QCD and LHCb data has been tabulated in Tab. 3.7. Our results are in good agreement with each bins as well.

Further semileptonic branching fraction is calculated by integrating the differential branching fractions and is compared with LHCb along with other theoretical approaches and it is observed that our results are well within the uncertainty presented in LFQM results [147], however our results overshoot in comparison with RQM [149] and pQCD [142] results for $\ell = e$ or μ mode. For $\ell = \tau$, our results match well with and are within uncertainty predicted by pQCD results. Uncertainty in branching fraction arises mainly due to the uncertainty in form factor which is transported to

Table 3.7: Normalized decay rates in terms of w bins in comparison with LQCD and LHCb data.

w bin	Present	LQCD [141]	LHCb [1]
1.0 - 1.1087	0.183 ± 0.019	0.187 (11)	0.183 (12)
1.1087 - 1.1688	0.146 ± 0.015	0.1507 (60)	0.144 (84)
1.1688 - 1.2212	0.133 ± 0.019	0.1371 (38)	0.148 (76)
1.2212 - 1.2717	0.127 ± 0.018	0.1296 (24)	0.128 (77)
1.2717 - 1.3226	0.123 ± 0.018	0.1230 (26)	0.117 (69)
1.3226 - 1.3814	0.130 ± 0.020	0.1275 (54)	0.122 (62)
1.3814 - 1.4667	0.157 ± 0.026	0.145 (15)	0.158 (93)

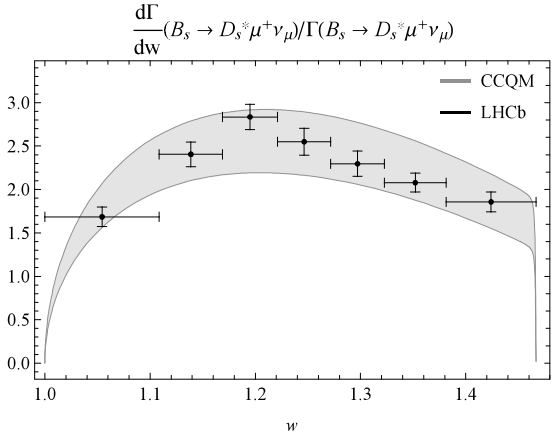

Figure 3.6: Normalized differential decay rates as a function of recoil parameter Eq. (3.16) for $B_s \to D_s^* \mu^+ \nu_\mu$ along with LHCb data [1]

Table 3.8: Branching fraction for $B_s \to D_s^{(*)-}$ transitions (in %)

Channel	Present	RQM [149]	LFQM [147]	LFQM [148]	pQCD [142]	LHCb [139]
$B_s^0 \to D_s^- e^+ \nu_e$	2.89 ± 0.50	2.1 ± 0.2	2.45 ± 0.27	- - -	$1.84^{+0.77}_{-0.51}$	- - -
$B_s^0 \to D_s^- \mu^+ \nu_\mu$	2.88 ± 0.49	- - -	- - -	- - -	- - -	$2.49 \pm 0.12 \pm 0.14 \pm 0.16$
$B_s^0 \to D_s^- \tau^+ \nu_\tau$	0.78 ± 0.15	0.62 ± 0.05	0.733 ± 0.081	- - -	$0.63^{+0.17}_{-0.13}$	- - -
$B_s^0 \to D_s^{*-} e^+ \nu_e$	6.42 ± 0.67	5.3 ± 0.5	6.05 ± 0.67	- - -	$4.42^{+1.27}_{-1.00}$	- - -
$B_s^0 \to D_s^{*-} \mu^+ \nu_\mu$	6.39 ± 0.67	- - -	- - -	$5.2^{+0.6}_{-0.6}$	- - -	$5.38 \pm 0.25 \pm 0.46 \pm 0.30$
$B_s^0 \to D_s^{*-} \tau^+ \nu_\tau$	1.53 ± 0.15	1.3 ± 0.1	1.51 ± 0.17	$1.3^{+0.2}_{-0.1}$	$1.20^{+0.26}_{-0.23}$	- - -

branching fraction. Propagation of uncertainty is explained in detail in Sec. 3.3. The comparison of computed branching fraction with other theoretical approaches as well as with LHCb data for $B_s \to D_s^{(*)} \ell \nu_\ell$ is displayed in Tab. 3.8. The differences in the result mainly arise due to the difference between the values of form factor used in RQM, pQCD and in our computations. It is important to emphasize that our result for $B_s^0 \to D_s^{(*)-} \mu^+ \nu_\mu$ channel are within the uncertainty predicted by LHCb collaboration [139]. We have also computed the ratio of decay width of the tau channel to the muon channel as a probe for lepton flavor universality (LFU) which are tabulated in Tab. 3.9. It shows that our result agree with LHCb and recent lattice data very well. Our results also match well with the $R(D_s^*)$ and $R(J/\psi)$ results calculated using the model given in Ref. [176, 177]. The most precise result for the ratio of decay widths is given by Belle Collaboration and the results are $R(D)$=0.307±0.037±0.016 and

Table 3.9: Ratio of semileptonic decay widths with heavy quark expansion (HQE), LHCb and Lattic QCD data

Ratio	$R(D_s) = \frac{\Gamma(B_s^0 \to D_s^- \tau^+ \nu_\tau)}{\Gamma(B_s^0 \to D_s^- \mu^+ \nu_\mu)}$	$R(D_s^*) = \frac{\Gamma(B_s^0 \to D_s^{*-} \tau^+ \nu_\tau)}{\Gamma(B_s^0 \to D_s^{*-} \mu^+ \nu_\mu)}$	$\frac{\Gamma(B_s^0 \to D_s^- \mu^+ \nu_\mu)}{\Gamma(B_s^0 \to D_s^{*-} \mu^+ \nu_\mu)}$
Present	0.271±0.069	0.240±0.034	0.451±0.096
HQE [144]	0.2971±0.0034	0.2472±0.0077	- - -
pQCD [142]	$0.341^{+0.024}_{-0.025}$	$0.271^{+0.015}_{-0.016}$	- - -
LQCD [140, 141]	$0.2993(46)$	$0.2442(79)_{latt}(35)_{EM}$	$0.429(43)_{latt}(4)_{EM}$
LHCb [139]	- - -	- - -	0.464±0.013±0.043

$R(D^*)$=0.283±0.018±0.014 [178]. It is also important to keep in mind that results on $R(D_s^*)$ calculated using CCQM are well within the uncertainty range presented by Belle Collaboration [178], whereas the mean value without considering the uncertainty is lower by 16% than the Belle results. Our results for the ratio of decay width of $B_s \to D_s$ and $B_s \to D_s^*$ for muon channel match well with LHCb and lattice data. This work has already been published in [179]. Results of other observables for $B_s \to D_s^{(*)-}$ semileptonic decay will be discussed in the next chapter.

3.5 $b \to d\ell^+\ell^-$ Transition

With the announcement of experimental results, the role of flavor changing neutral current (FCNC) decay $b \to s$ has gathered a lot of importance in the search of New Physics(NP) as well as a probe to test the predictions of standard model (SM). Experimental results for $B \to K^{(*)}\ell^+\ell^-$ and $B \to D^{(*)}\ell^+\nu_\ell$ [180–185] decay have been observed to violate lepton flavor universality (LFU) on the account of deviation from the standard model predictions [186–192]. Another important probe could be the $b \to d\ell^+\ell^-$ decay as same FCNC scenario is followed in this decay at quark level [193, 194]. As within SM the branching fraction for $b \to d\ell^+\ell^-$ is suppressed by a factor of $|V_{td}/V_{ts}|^2$, $b \to d\ell^+\ell^-$ decay is not much explored as compared to $b \to s\ell^+\ell^-$ processes. These transitions were first observed by LHCb for the channel $B^+ \to \pi^+\mu^+\mu^-$ [42] and in $\Lambda_b^0 \to p\mu^+\mu^-$ [195]. Recently, the evidence for

$B_s^0 \to \bar{K}^{*0}\mu^+\mu^-$ channel has been published by LHCb with the significance of 3.4σ which is given by

$$\mathcal{B}(B^+ \to \pi^+\mu^+\mu^-) = (1.83 \pm 0.24 \pm 0.05) \times 10^{-8}$$

$$\mathcal{B}(B_s^0 \to \bar{K}^*(892)^0\mu^+\mu^-) = (2.9 \pm 1.0 \pm 0.3 \pm 0.3) \times 10^{-8}$$

Recently the Belle collaboration has also reported the branching fraction for the $B^+ \to \pi^+\pi^-\ell^+\ell^-$ channel [44]. Details for several theoretical studies investigating the $b \to d$ transition is given in Sec. 1.1. On top of that, form factors for $B \to \pi, \rho, K^{(*)}$ channel were calculated using LCSR [7, 9, 47–51, 175]. Semileptonic form factors obtained using Lattice calculations are reported in [52–54]. The important ratio for the probe of New Physics(NP) beyond the standard model could be the ratio of $b \to s\ell^+\ell^-$ to $b \to d\ell^+\ell^-$ as it tests the flavor dynamics of the interactions involved and allows to look for minimum flavor violation [196, 197]. This ratio was experimentally calculated at LHCb collaboration for the channel $B^+ \to \pi^+$ and $B^+ \to K^+$ [42]. The ratio of branching fraction for channels $B_s^0 \to \bar{K}^*(892)^0$ and $B^0 \to K^*(892)^0$ was calculated along with two body decays of B_s meson [198].

Here, the rare decay associated with $b \to d$ transition for channels $B^{+(0)} \to (\pi^{+(0)}, \rho^{+(0)}, w)\ell^+\ell^-$ and $B_s^0 \to \bar{K}^{(*)0}\ell^+\ell^-$ where $\ell = e, \mu, \tau$ has been investigated using CCQM within the framework of the standard model, where form factors are calculated in the entire q^2 range. Various physical observables like branching fraction, forward-backward asymmetry, longitudinal polarization and few angular observables are computed using form factors. We have also computed the ratios of branching fraction for $b \to s$ to $b \to d$ decays. We provide the comparison of our calculated result with results from other theoretical approaches and available theoretical results.

Table 3.10: Masses, total widths and dilepton decay widths of vector resonance states [12]

State	Mass (MeV)	Γ_V (MeV)	$\mathcal{B}(V \to \ell^+\ell^-)$
ρ	775.26	147.8	4.63×10^{-5}
ω	785.65	8.49	7.38×10^{-5}
ϕ	1.019	4.249	2.94×10^{-4}
J/ψ	3096.900	92.9 $\times 10^{-3}$	5.96×10^{-2}
$\psi(2S)$	3686.10	294 $\times 10^{-3}$	7.96×10^{-3}

3.5.1 Effective Hamiltonian

The effective Hamiltonian for rare $b \to d\ell^+\ell^-$ decay can be written in terms of operator product expansion as [13, 199, 200]

$$\mathcal{H}_{eff}^{SM} = -\frac{4G_F}{\sqrt{2}} V_{td}^* V_{tb} \left[\sum_{i=1}^{10} C_i(\mu)\mathcal{O}_i(\mu) + \lambda_u^* \sum_{i=1}^{2} C_i(\mu)[\mathcal{O}_i(\mu) - \mathcal{O}_i^{(u)}] \right] \tag{3.17}$$

where $\lambda_u \equiv \frac{V_{ub}^* V_{ud}}{V_{tb}^* V_{td}}$, C_i denotes the Wilson coefficients and $\mathcal{O}_i$ are the set of local operators. For $b \to d\ell^+\ell^-$ transition, the local operators within the framework of SM can be defined as [13, 200].

$$\begin{aligned}
&\mathcal{O}_1^u = (\bar{d}_{a_1}\gamma^\mu P_L u_{a_2})(\bar{u}_{a_2}\gamma_\mu P_L b_{a_1}), && \mathcal{O}_2^u = (\bar{d}\gamma^\mu P_L u)(\bar{u}\gamma_\mu P_L b),\\
&\mathcal{O}_1 = (\bar{d}_{a_1}\gamma^\mu P_L c_{a_2})(\bar{c}_{a_2}\gamma_\mu P_L b_{a_1}), && \mathcal{O}_2 = (\bar{d}\gamma^\mu P_L c)(\bar{c}\gamma_\mu P_L b),\\
&\mathcal{O}_3 = (\bar{d}\gamma^\mu P_L b)\textstyle\sum_q(\bar{q}\gamma_\mu P_L q), && \mathcal{O}_4 = (\bar{d}_{a_1}\gamma^\mu P_L b_{a_2})\textstyle\sum_q(\bar{q}_{a_2}\gamma_\mu P_L q_{a_1}),\\
&\mathcal{O}_5 = (\bar{d}\gamma^\mu P_L b)\textstyle\sum_q(\bar{q}\gamma_\mu P_R q), && \mathcal{O}_6 = (\bar{d}_{a_1}\gamma^\mu P_L b_{a_2})\textstyle\sum_q(\bar{q}_{a_2}\gamma_\mu P_R q_{a_1}),\\
&\mathcal{O}_7 = \tfrac{e}{16\pi^2}\bar{m}_b\,(\bar{d}\sigma^{\mu\nu}P_R b)F_{\mu\nu}, && \mathcal{O}_8 = \tfrac{g}{16\pi^2}\bar{m}_b\,(\bar{d}_{a_1}\sigma^{\mu\nu}P_R T_{a_1 a_2} b_{a_2})G_{\mu\nu},\\
&\mathcal{O}_9 = \tfrac{e^2}{16\pi^2}(\bar{d}\gamma^\mu P_L b)(\bar{\ell}\gamma_\mu \ell), && \mathcal{O}_{10} = \tfrac{e^2}{16\pi^2}(\bar{d}\gamma^\mu P_L b)(\bar{\ell}\gamma_\mu\gamma_5 \ell),
\end{aligned} \tag{3.18}$$

Table 3.11: Values of the input parameters [13] and SM Wilson coefficients [14]. Values of masses are in GeV

m_W	$\sin^2\theta_W$	$\alpha(M_Z)$	$\bar{m}_c$	$\bar{m}_b$	$\bar{m}_t$	C_{10}	C_9
80.41	0.2313	1/128.94	1.27	4.68	173.3	-4.410	4.232
C_1	C_2	$C_3(\%)$	$C_4(\%)$	$C_5(\%)$	$C_6(\%)$	C_7	C_8
-0.175	1.076	1.258	-3.279	1.112	-3.634	-0.302	-0.148

Here $G_{\mu\nu}$ and $F_{\mu\nu}$ describe gluon and photon field strengths respectively. a_1,a_2 are color indices and $T_{a_1 a_2}$ serves as the generator for $SU(3)$ color group. a_1,a_2 are not mentioned for color singlet currents. $P_{L,R}$ are the projection operators and renormalization scale factor is chosen to be μ. $\mathcal{O}_{1,2}$ are current-current, $\mathcal{O}_{3-6}$ are QCD penguin, $\mathcal{O}_{7,8}$ are dipole and $\mathcal{O}_{9,10}$ are semileptonic electroweak penguin operators. In order to distinguish QCD quark masses from constituent quark masses we use bar symbol for QCD quark masses. The matrix-element for $b \to d\ell^+\ell^-$ transition can be written as [199, 200]

$$\mathcal{M}(b \to d\ell^+\ell^-) = \frac{G_F \alpha}{\sqrt{2}\pi} V_{tb}^* V_{td} \Bigg\{ C_9^{\text{eff}} (\bar{d}\gamma_\mu P_L b)(\bar{\ell}\gamma^\mu \ell) + C_{10}(\bar{d}\gamma_\mu P_L b)(\bar{\ell}\gamma^\mu\gamma_5 \ell) - \frac{2\bar{m}_b}{q^2} C_7^{\text{eff}} \left(\bar{d} i\sigma_{\mu\nu} q_\nu P_R b\right)(\bar{\ell}\gamma^\mu \ell) \Bigg\} \tag{3.19}$$

where the effective Wilson coefficients are given by [2, 201]

$$C_7^{\text{eff}}(\mu) = C_7(\mu) + i\alpha_s \left\{ \frac{2}{9} \left(\frac{\alpha_s(m_W)}{\alpha_s(\mu)} \right)^{14/23} [G_I(x_t) - 0.1687] - 0.03 C_2(\mu) \right\} \tag{3.20}$$

with $x_t = m_t^2/m_W^2$ and

$$G_I(x_t) = \frac{x_t(x_t^2 - 5x_t - 2)}{8(x_t - 1)^3} + \frac{3x_t^2 \ln\, x_t}{4(x_t - 1)^4}.$$

The correction in the four-quark operator $\mathcal{O}_{1,2}^u$ and $\mathcal{O}_{1-6}$ in Eq. (3.17) is contained

by $C_9^{\rm eff}(\mu)$ and which can be written as [2, 201–208]

$$C_9^{\rm eff}(\mu) = \xi_1 + |V_{tb}^* V_{td}|\xi_2, \tag{3.21}$$

where

$$\begin{aligned}\xi_1 = C_9 + C_0 h^{\rm eff}(\hat{m}_c, \hat{s}) - \frac{1}{2}h(1,\hat{s})(4C_3 + 4C_4 + 3C_5 + C_6) \\ -\frac{1}{2}h(0,\hat{s})(C_3 + 3C_4) + \frac{2}{9}(3C_3 + C_4 + 3C_5 + C_6)\end{aligned} \tag{3.22}$$

$$\xi_2 = \Big[h^{\rm eff}(\hat{m}_c, \hat{s}) - h^{\rm eff}(\hat{m}_u, \hat{s})\Big](3C_1 + C_2) \tag{3.23}$$

where $C_0 \equiv 3C_1 + C_2 + 3C_3 + C_4 + 3C_5 + C_6$ and the quark-loop function is given by

$$h(\hat{m}_q, \hat{s}) = -\frac{8}{9}\ln \hat{m}_q + \frac{8}{27} + \frac{4}{9}x - \frac{2}{9}(2+x)|1-x|^{1/2} \begin{cases} \left(\ln\left|\frac{\sqrt{1-x}+1}{\sqrt{1-x}-1}\right| - i\pi\right), & \text{for } x \equiv \frac{4\hat{m}_q^2}{\hat{s}} < 1, \\ 2\arctan\frac{1}{\sqrt{x-1}}, & \text{for } x \equiv \frac{4\hat{m}_q^2}{\hat{s}} > 1, \end{cases}$$

and

$$h(0, \hat{s}) = \frac{8}{27} - \frac{4}{9}\ln \hat{s} + \frac{4}{9}i\pi,$$

further the functions,

$$\begin{aligned} h^{\rm eff}(\hat{m}_c, \hat{s}) &= h(\hat{m}_c, \hat{s}) + \frac{3\pi}{\alpha^2 C_0}\sum_{V=J/\psi,\psi(2S),\ldots} \frac{m_V \mathcal{B}(V\to\ell^+\ell^-)\Gamma_V}{m_V^2 - q^2 - i m_V \Gamma_V}, \\ h^{\rm eff}(\hat{m}_u, \hat{s}) &= h(\hat{m}_u, \hat{s}) + \frac{3\pi}{\alpha^2 C_0}\sum_{V=\rho^0,\omega,\phi} \frac{m_V \mathcal{B}(V\to\ell^+\ell^-)\Gamma_V}{m_V^2 - q^2 - i m_V \Gamma_V} \end{aligned} \tag{3.24}$$

where $\hat{m}_q = \bar{m}_q/m_1$, $\hat{s} = q^2/m_1^2$. The Eq. (3.24) contains terms which describes vector resonances, nonresonant contribution is obtained by omitting those terms. The inputs for mass, total decay width and dilepton branching fractions are taken from PDG [12] which are displayed in Tab. 3.10 The value of $\mu = \bar{m}_{b\,\rm pole}$ is used for the renormalization scale. The next-to-leading order SM Wilson coefficients are employed from Ref. [14] at the value of renormalization scale $\mu_b = 4.8$ GeV. Tab. 3.11 lists all inputs for the model independent parameters and Wilson coefficients.

The form factors for $B_{(s)} \to (\pi, \bar{K}^0, \rho, \omega^0, \bar{K}^{*0})\ell^+\ell^-$ channel in CCQM formalism is defined as in Eq. 3.6 − 3.9.

Here quark masses and meson size parameters are fitted with leptonic decay widths, with experimental data or with data from the lattice simulations and any differences are treated as the absolute uncertainty. At maximum recoil, the uncertainties are found to be less than 10%, and these are then transported to calculate form factors. Updated least square fitting method is performed to obtain the model parameter for present calculations [176, 209, 210]. Form factors for $B_{(s)} \to (\pi, \bar{K}^0, \rho, \omega^0, \bar{K}^{*0})\ell^+\ell^-$ channels are calculated using the *FORTRAN* and *Mathematica* code using the model parameters defined in Tab. 2.2. Computed form factors are given in Fig. 3.7. Double-pole representation of the Form factors is given by Eq. (3.10). Parameters of double pole approximation are given in Tab. 3.12 for different decay channels and it is important to note that the relative error for all the form factors is less than 1% in entire q^2 range.

Now using the data for model parameter Tab. 2.2, Wilson coefficients Tab. 3.11 and form factor Tab. 3.12, the branching fraction for rare $b \to d\ell^+\ell^-$ decay has been computed by integrating Eq. (3.25) over the full q^2 range.

$$\frac{d\Gamma(b \to d\ell^+\ell^-)}{dq^2} = \frac{G_F^2}{(2\pi)^3}\left(\frac{\alpha|V_{tb}^* V_{td}|}{2\pi}\right)^2 \frac{|\mathbf{p_2}|q^2\beta_\ell}{12m_1^2}\mathcal{H}_{\rm tot} \tag{3.25}$$

where

$$H_{tot} = \frac{1}{2}(\mathcal{H}_U^{11} + \mathcal{H}_U^{22} + \mathcal{H}_L^{11} + \mathcal{H}_L^{22}) + \delta_{\ell\ell}\left(\frac{1}{2}\mathcal{H}_U^{11} - \mathcal{H}_U^{22} + \frac{1}{2}\mathcal{H}_L^{11} - \mathcal{H}_L^{22} + \frac{3}{2}\mathcal{H}_S^{22}\right) \tag{3.26}$$

In what follows, $m_1 = m_{B_{(s)}}$ and m_2 is the mass of daughter mesons, $\beta_\ell = \sqrt{1 - 4m_\ell^2/q^2}$, $\delta_{\ell\ell} = 2m_\ell^2/q^2$ is the helicity flip suppression factor. Hence in the rest frame of $B_{(s)}$, $|\mathbf{p_2}| = \lambda^{1/2}(m_1^2, m_2^2, q^2)/(2\,m_1)$ is the momentum of the daughter meson with the Källen function $\lambda(a, b, c) = a^2 + b^2 + c^2 - 2(ab + bc + ca)$. The bilinear combinations of the helicity structure function given by Eq. (3.26) for $B_{(s)}^{(0)} \to \pi, \bar{K}^0$ decay channels are defined as [126],

$$\mathcal{H}_U^{ii} = 0, \qquad \mathcal{H}_L^{ii} = |H_0^i|^2, \qquad \mathcal{H}_S^{ii} = |H_{t0}^i|^2.$$

Table 3.12: Form factors and double pole parameters for $B \to (\pi, \rho, \omega)\ell^+\ell^-$ transitions

F	$F(0)$	a	b
$F_+^{B\to\pi}$	0.283 ± 0.019	1.294	0.349
$F_-^{B\to\pi}$	-0.238 ± 0.016	1.323	0.374
$F_T^{B\to\pi}$	0.268 ± 0.018	1.292	0.346
$A_+^{B\to\rho}$	0.227 ± 0.018	1.355	0355
$A_-^{B\to\rho}$	-0.240 ± 0.019	1.415	0.404
$A_0^{B\to\rho}$	0.319 ± 0.026	0.528	-0.295
$V^{B\to\rho}$	0.259 ± 0.021	1.472	0.452
$a_+^{B\to\rho}$	0.233 ± 0.019	1.362	0.360
$a_0^{B\to\rho}$	0.233 ± 0.019	0.575	-0.254
$g^{B^+\to\rho^+}$	0.233 ± 0.019	1.477	0.457
$A_+^{B^0\to\omega}$	0.206 ± 0.016	1.390	0.375
$A_-^{B^0\to\omega}$	-0.214 ± 0.017	1.442	0.417
$A_0^{B^0\to\omega}$	0.288 ± 0.023	0.557	-0.325
$V^{B^0\to\omega}$	0.229 ± 0.023	1.504	0.472
$a_+^{B^0\to\omega}$	0.206 ± 0.017	1.401	0.384
$a_0^{B^0\to\omega}$	0.206 ± 0.017	0.618	-0.275
$g^{B^0\to\omega}$	0.206 ± 0.017	1.506	0.472

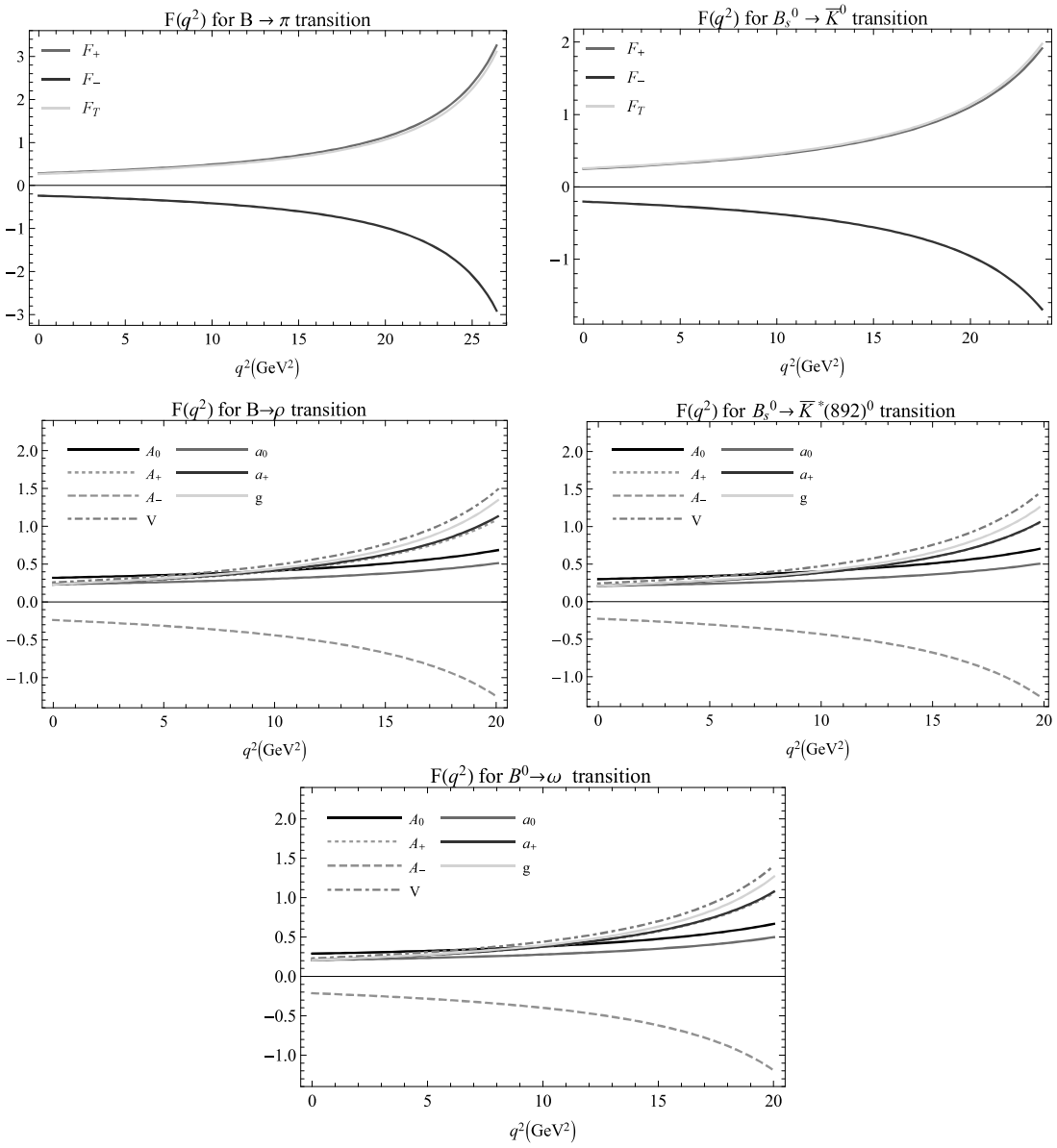

Figure 3.7: Form factors for $B \to (\pi, \rho, \omega)$ and $B_s \to (K, K^*)$ transitions

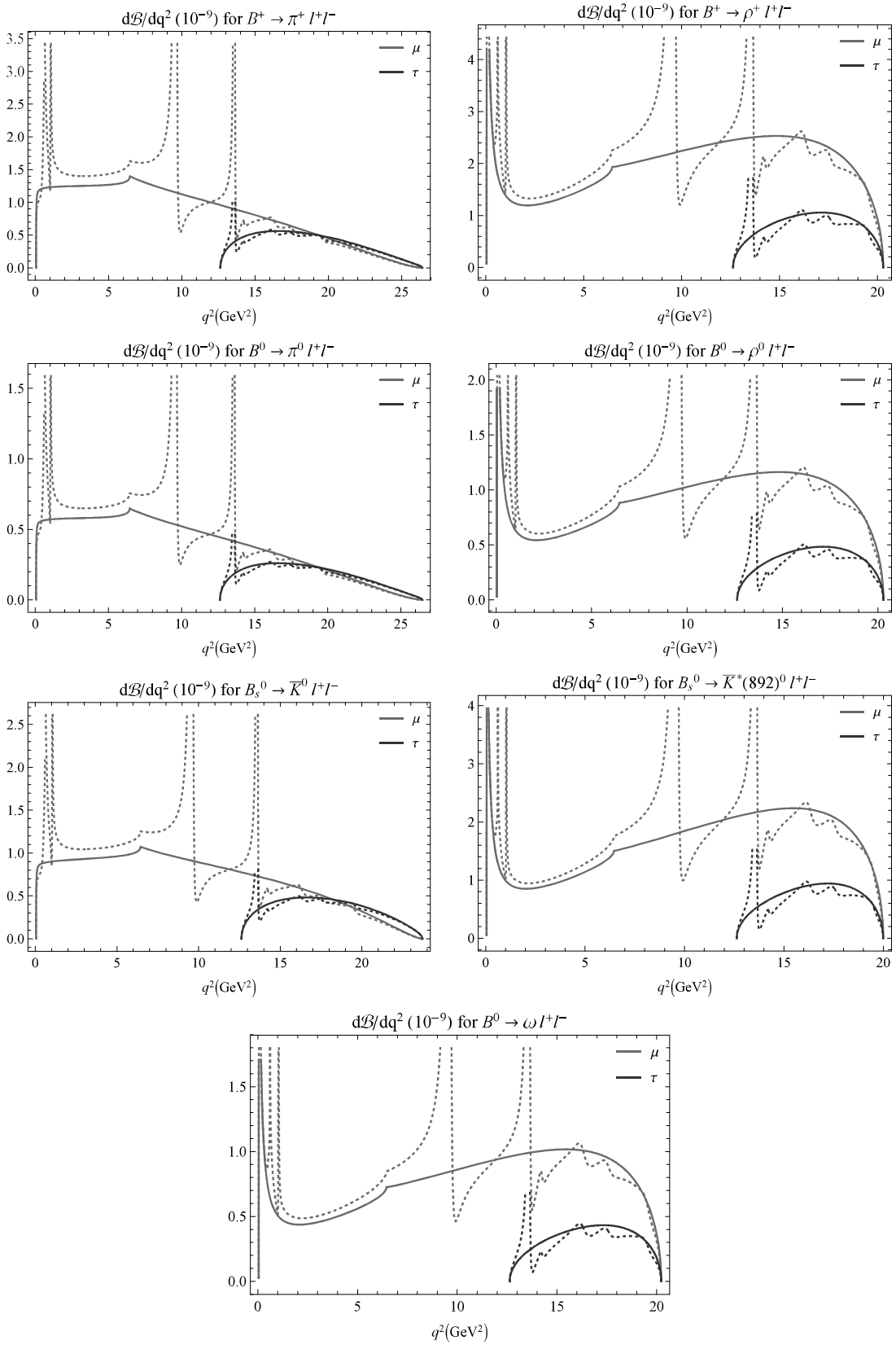

Figure 3.8: Differential branching fractions (solid lines - excluding resonances, dashed lines - including vector resonances) for $B \to (\pi, \rho, \omega)$ and $B_s \to (K, K^*)$ transitions.

The helicity amplitudes in terms of form factors are expressed as,

$$\begin{aligned} H_0^i &= \frac{2m_1|\mathbf{p_2}|}{\sqrt{q^2}}\mathcal{F}_+^i, \\ H_{t0}^i &= \frac{1}{\sqrt{q^2}}((m_1^2-m_2^2)\mathcal{F}_+^i + q^2\mathcal{F}_-^i) \end{aligned} \tag{3.27}$$

and the form factors $\mathcal{F}_{+-}^i$ for $i=1,2$ are related to form factors Eq. (3.6) − (3.9) as

$$\begin{aligned} \mathcal{F}_+^1 &= C_9^{\rm eff}F_+ + C_7^{\rm eff}F_T\frac{2\bar{m}_b}{m_1+m_2}, \\ \mathcal{F}_-^1 &= C_9^{\rm eff}F_- - C_7^{\rm eff}F_T\frac{2\bar{m}_b}{m_1+m_2}\frac{m_1^2-m_2^2}{q^2}, \\ \mathcal{F}_+^2 &= C_{10}F_+ \quad , \qquad \mathcal{F}_-^2 = C_{10}F_-. \end{aligned} \tag{3.28}$$

Similarly, the bilinear combinations of the helicity structure function for $B_{(s)}^{(0)} \to \rho, \omega, \bar{K}^*(892)^0$ decay channels are defined as [126],

$$\mathcal{H}_U^{ii} = |H_{+1+1}^i|^2 + |H_{-1-1}^i|^2, \qquad \mathcal{H}_L^{ii} = |H_{00}^i|^2, \qquad \mathcal{H}_S^{ii} = |H_{t0}^i|^2$$

where the helicity amplitudes are expressed via the form factors appearing in the matrix element of the $b \to d\ell^+\ell^-$ rare decay as

$$\begin{aligned} H_{t0}^i &= \frac{1}{m_1+m_2}\frac{m_1\,|\mathbf{p_2}|}{m_2\sqrt{q^2}}\left(Pq\,(-A_0^i + A_+^i) + q^2 A_-^i\right), \\ H_{\pm1\pm1}^i &= \frac{1}{m_1+m_2}\left(-Pq\,A_0^i \pm 2\,m_1\,|\mathbf{p_2}|\,V^i\right), \\ H_{00}^i &= \frac{1}{m_1+m_2}\frac{1}{2\,m_2\sqrt{q^2}} \times \left(-Pq\,(m_1^2-m_2^2-q^2)\,A_0^i + 4\,m_1^2\,|\mathbf{p_2}|^2\,A_+^i\right). \end{aligned} \tag{3.29}$$

The relation between form factors A^i and V^i $(i=1,2)$ and transition form factors for

the $b \to d$ transition Eq. (3.6) and (3.8) is given in the following manner

$$\begin{aligned}
V^{(1)} &= C_9^{\rm eff}\, V + C_7^{\rm eff}\, g\, \frac{2\bar{m}_b(m_1+m_2)}{q^2}\,, \\
A_0^{(1)} &= C_9^{\rm eff}\, A_0 + C_7^{\rm eff}\, a_0\, \frac{2\bar{m}_b(m_1+m_2)}{q^2}\,, \\
A_+^{(1)} &= C_9^{\rm eff}\, A_+ + C_7^{\rm eff}\, a_+\, \frac{2\bar{m}_b(m_1+m_2)}{q^2}\,, \\
A_-^{(1)} &= C_9^{\rm eff}\, A_- + C_7^{\rm eff}\, (a_0-a_+)\, \frac{2\bar{m}_b(m_1+m_2)}{q^2}\, \frac{Pq}{q^2}\,, \\
V^{(2)} &= C_{10}\, V, \qquad A_0^{(2)} = C_{10}\, A_0, \qquad A_\pm^{(2)} = C_{10}\, A_\pm.
\end{aligned} \tag{3.30}$$

After helicity structure functions are defined, we now plot the differential branching fractions calculated using Eq. 3.25 in Fig. 3.8. By computing numerical integration of Fig. 3.8, the rare branching fractions are calculated and displayed in Tab. 3.13 − 3.14.

The branching fractions corresponding to $b \to d\nu\bar{\nu}$ decays are calculated. The differential branching fractions are defined as [126]

$$\frac{d\Gamma(b\to d\nu\bar{\nu})}{dq^2} = \frac{G_F^2}{(2\pi)^3}\Big(\frac{\alpha|V_{tb}^*V_{td}|}{2\pi}\Big)^2 \left[\frac{D_\nu(x_t)}{\sin^2\theta_W}\right]^2 \frac{|\mathbf{p_2}|\,q^2}{4m_{B,B_s}^2} \times (H_U + H_L), \tag{3.31}$$

where $x_t = \bar{m}_t^2/m_W^2$ and the function D_ν with α_s correction is given by [214]

$$D_\nu(x) = D_0(x) + \frac{\alpha_s}{4\pi} D_1(x) \tag{3.32}$$

with

$$D_0(x) = \frac{x}{8}\left(\frac{2+x}{x-1} + \frac{3x-6}{(x-1)^2}\,\ln x\right) \tag{3.33}$$

and

$$\begin{aligned}
D_1(x) &= -\frac{29x - x^2 - 4x^3}{3(1-x)^2} - \frac{x + 9x^2 - x^3 - x^4}{(1-x)^3}\,\ln x \\
&+ \frac{8x + 4x^2 + x^3 - x^4}{2(1-x)^3}\,\ln^2 x - \frac{4x - x^3}{(1-x)^2}\int_1^x dt \frac{\ln t}{1-t} \\
&+ 8x\frac{\partial D_0(x)}{\partial x}\,\ln\left(\frac{\mu_b^2}{m_W^2}\right).
\end{aligned} \tag{3.34}$$

Table 3.13: Branching fractions of $B \to (\pi, \rho, \omega)$ transitions

Channel	Nonresonant	Resonant	LCSR [7]	RQM [3, 211]	Exp. [12]
$10^8\mathcal{B}(B^+ \to \pi^+ e^+ e^-)$	2.18 ± 0.30	1.82 ± 0.18	$1.89^{+0.23}_{-0.22}$	- - -	< 8.0
$10^8\mathcal{B}(B^+ \to \pi^+ \mu^+ \mu^-)$	2.17 ± 0.30	1.81 ± 0.18	$1.88^{+0.24}_{-0.21}$	2.0 ± 0.2	$1.83 \pm 0.24 \pm 0.05$ [212]
$10^8\mathcal{B}(B^+ \to \pi^+ \tau^+ \tau^-)$	0.53 ± 0.15	0.41 ± 0.12	$0.90^{+0.13}_{-0.12}$	0.70 ± 0.07	- - -
$10^7\mathcal{B}(B^+ \to \pi^+ \nu\bar{\nu})$	0.74 ± 0.10	- - -	- - -	1.2 ± 0.1	< 140
$10^8\mathcal{B}(B^0 \to \pi^0 e^+ e^-)$	1.01 ± 0.14	0.84 ± 0.08	$0.87^{+0.11}_{-0.10}$	- - -	< 8.4
$10^8\mathcal{B}(B^0 \to \pi^0 \mu^+ \mu^-)$	1.01 ± 0.14	0.84 ± 0.08	$0.87^{+0.11}_{-0.10}$	- - -	< 6.9
$10^8\mathcal{B}(B^0 \to \pi^0 \tau^+ \tau^-)$	0.24 ± 0.07	0.19 ± 0.06	0.41 ± 0.06	- - -	- - -
$10^7\mathcal{B}(B^0 \to \pi^0 \nu\bar{\nu})$	0.34 ± 0.05	- - -	- - -	- - -	< 90
$10^8\mathcal{B}(B^+ \to \rho^+ e^+ e^-)$	4.82 ± 2.39	3.70 ± 1.34	4.0 ± 0.4	- - -	- - -
$10^8\mathcal{B}(B^+ \to \rho^+ \mu^+ \mu^-)$	4.05 ± 1.45	2.94 ± 0.94	3.9 ± 0.4	4.4 ± 0.5	- - -
$10^8\mathcal{B}(B^+ \to \rho^+ \tau^+ \tau^-)$	0.63 ± 0.14	0.43 ± 0.09	0.40 ± 0.04	0.75 ± 0.08	- - -
$10^7\mathcal{B}(B^+ \to \rho^+ \nu\bar{\nu})$	1.45 ± 0.38	- - -	- - -	2.9 ± 0.3	< 300
$10^7\mathcal{B}(B^+ \to \rho^+ \gamma)$	8.55 ± 1.38	- - -	$13.8^{+1.6}_{-1.5}$	- - -	9.8 ± 2.5
$10^8\mathcal{B}(B^0 \to \rho^0 e^+ e^-)$	2.21 ± 1.09	1.70 ± 0.61	1.9 ± 0.2	- - -	- - -
$10^8\mathcal{B}(B^0 \to \rho^0 \mu^+ \mu^-)$	1.86 ± 0.66	1.35 ± 0.43	1.8 ± 0.2	- - -	- - -
$10^8\mathcal{B}(B^0 \to \rho^0 \tau^+ \tau^-)$	0.29 ± 0.06	0.20 ± 0.04	0.2 ± 0.02	- - -	- - -
$10^7\mathcal{B}(B^0 \to \rho^0 \nu\bar{\nu})$	0.67 ± 0.18	- - -	- - -	- - -	< 400
$10^7\mathcal{B}(B^0 \to \rho^0 \gamma)$	3.96 ± 0.64	- - -	6.4 ± 0.7	- - -	- - -
$10^8\mathcal{B}(B^0 \to \omega e^+ e^-)$	1.85 ± 0.89	1.41 ± 0.59	1.3 ± 0.1	- - -	- - -
$10^8\mathcal{B}(B^0 \to \omega \mu^+ \mu^-)$	1.57 ± 0.55	1.14 ± 0.44	1.2 ± 0.1	- - -	- - -
$10^8\mathcal{B}(B^0 \to \omega \tau^+ \tau^-)$	0.25 ± 0.05	0.18 ± 0.03	0.13 ± 0.01	- - -	- - -
$10^7\mathcal{B}(B^0 \to \omega \nu\bar{\nu})$	0.56 ± 0.15	- - -	- - -	- - -	< 400
$10^7\mathcal{B}(B^0 \to \omega \gamma)$	3.11 ± 0.50	- - -	$5.8^{+0.6}_{-0.7}$	- - -	- - -

Table 3.14: Branching fractions of $B_s \to K/K^*$ transitions

Channel	Nonresonant	Resonant	LCSR [7]	RQM [3, 211]	Exp.
$10^8\mathcal{B}(B_s^0 \to \bar{K}^*(892)^0 e^+e^-)$	3.91 ± 1.47	2.95 ± 0.80	4.0 ± 0.4	- - -	- - -
$10^8\mathcal{B}(B_s^0 \to \bar{K}^*(892)^0 \mu^+\mu^-)$	3.32 ± 0.94	2.36 ± 0.57	3.8 ± 0.3	4.2 ± 0.4	$2.9 \pm 1.0 \pm 0.2 \pm 0.3$ [213]
$10^8\mathcal{B}(B_s^0 \to \bar{K}^*(892)^0 \tau^+\tau^-)$	0.53 ± 0.10	0.37 ± 0.06	0.50 ± 0.04	0.75 ± 0.08	- - -
$10^7\mathcal{B}(B_s^0 \to \bar{K}^*(892)^0 \nu\bar{\nu})$	1.19 ± 0.25	- - -	- - -	- - -	- - -
$10^7\mathcal{B}(B_s^0 \to \bar{K}^*(892)^0 \gamma)$	6.66 ± 0.96	- - -	$12.0^{+1.1}_{-1.2}$	3.0 ± 0.3	- - -
$10^8\mathcal{B}(B_s^0 \to \bar{K}^0 e^+e^-)$	1.65 ± 0.21	1.35 ± 0.12	$1.99^{+0.21}_{-0.20}$	- - -	- - -
$10^8\mathcal{B}(B_s^0 \to \bar{K}^0 \mu^+\mu^-)$	1.64 ± 0.21	1.35 ± 0.12	$1.99^{+0.21}_{-0.20}$	2.2 ± 0.2	- - -
$10^8\mathcal{B}(B_s^0 \to \bar{K}^0 \tau^+\tau^-)$	0.39 ± 0.09	0.30 ± 0.08	0.74 ± 0.07	0.55 ± 0.06	- - -
$10^7\mathcal{B}(B_s^0 \to \bar{K}^0 \nu\bar{\nu})$	0.55 ± 0.07	- - -	- - -	1.41 ± 0.14	- - -

The associated bilinear helicity combinations for the channels $B_{(s)}^{(0)} \to \pi, \bar{K}^0$ can be expressed as

$$\mathcal{H}_L = |H_0|^2, \qquad \mathcal{H}_U = 0 \tag{3.35}$$

with

$$H_0 = \frac{2m_1|\mathbf{p}_2|}{\sqrt{q^2}} F_+. \tag{3.36}$$

Similarly, the bilinear helicity combinations for the channels $B_{(s)}^{(0)} \to \rho, \omega, \bar{K}^*(892)^0$ can be written as

$$\mathcal{H}_U = |H_{+1+1}|^2 + |H_{-1-1}|^2, \qquad \mathcal{H}_L = |H_{00}|^2, \tag{3.37}$$

with

$$\begin{aligned} H_{\pm 1 \pm 1} &= \frac{1}{m_1 + m_2} \left(-Pq\, A_0 \pm 2\, m_1\, |\mathbf{p_2}|\, V\right), \\ H_{00} &= \frac{1}{m_1 + m_2} \frac{1}{2\, m_2 \sqrt{q^2}} \times \left(-Pq\, (m_1^2 - m_2^2 - q^2)\, A_0 + 4\, m_1^2\, |\mathbf{p_2}|^2\, A_+\right). \end{aligned} \tag{3.38}$$

To compute the branching fraction defined in Eq. (3.31), the required values of form

factors (F_+, $A_{0,+,-}$ and V) defined in Eq. (3.36) and (3.39) are taken from Tab. 3.12. Finally, the radiative decay width $B_{(s)}^{(0)} \to (\rho, \omega, \bar{K}^*(892)^0)\gamma$ has been computed using the relation

$$\Gamma(B_{(s)}^{(0)} \to (\rho, \omega, \bar{K}^*(892)^0)\gamma) = \frac{G_F^2 \alpha |V_{tb}V_{td}^*|^2}{32\pi^4} \bar{m}_b^2 m_1^3 \times \left(1 - \frac{m_2^2}{m_1^2}\right)^3 |C_7^{\text{eff}}|^2 \, g^2(0).$$

where, α is the electromagnetic coupling constant (Tab. 3.11).

3.5.2 Results and Discussion

Using the model parameters in Tab. 2.2, we calculate the transition form factors given in Eq. (3.6) − (3.8) in the entire range of momentum transfer and depicted in Fig. 3.7. A superscript ^{c} is used to differentiate them from our regular form factors. Those relations are given by

$$\begin{aligned} F_0^c &= F_+ + \frac{q^2}{m_1^2 - m_2^2} F_-, \qquad (3.39) \\ A_0 &= \frac{m_1 + m_2}{m_1 - m_2} A_1^c, \quad A_+ = A_2^c, \\ A_- &= \frac{2m_2(m_1 + m_2)}{q^2}(A_3^c - A_0^c), \quad V = V^c, \\ a_0 &= T_2^c, \quad g = T_1^c, \\ a_+ &= T_2^c + \frac{q^2}{m_1^2 - m_2^2} T_3^c. \qquad (3.40) \end{aligned}$$

Additionally, we also note that the form factors Eq. (3.40) satisfy the constraints

$$\begin{aligned} A_0^c(0) &= A_3^c(0) \qquad (3.41) \\ 2m_2 A_3^c(q^2) &= (m_1 + m_2) A_1^c(q^2) - (m_1 - m_2) A_2^c(q^2). \end{aligned}$$

Since $a_0(0) = a_+(0) = g(0)$, we present the form factors $A_0^c(0) = (m_1 - m_2)[A_0(0) - A_+(0)]/(2m_2)$, $A_1^c(0) = A_0(0)(m_1 - m_2)/(m_1 + m_2)$, $A_2^c(0) = A_+(0)$, $T_1^c(0) = g(0)$ and $T_3^c(0) = \lim_{q^2 \to 0}(m_1^2 - m_2^2)(a_+ - a_0)/q^2$ obtained in our model and compare them with those from other approaches. Here the superscript is omitted for simplification and we will also not use it while comparing with other approaches.

Table 3.15: Form factor for $B \to \pi$ transitions at maximum recoil

Theory	$B \to \pi$	
	$f_{+,0}(0)$	$f_T(0)$
Present	0.283 ± 0.019	0.268 ± 0.018
LCSR [47]	0.280	0.260
LCSR [7]	$0.285^{+0.016}_{-0.015}$	$0.267^{+0.015}_{-0.014}$
LCSR [48]	0.301 ± 0.023	0.273 ± 0.021
LCSR [49]	0.21 ± 0.07	- - -
SUSY [5]	0.258	- - -
pQCD [2]	$0.26^{+0.04}_{-0.03} \pm 0.03 \pm 0.02$	$0.26^{+0.04}_{-0.03} \pm 0.03 \pm 0.02$
pQCD [14]	- - -	- - -
SCET [167]	0.247	0.253
RQM [3, 4]	0.217 ± 0.011	0.240 ± 0.012
CQM [6]	0.29	0.28
LFQM [8]	0.25	- - -

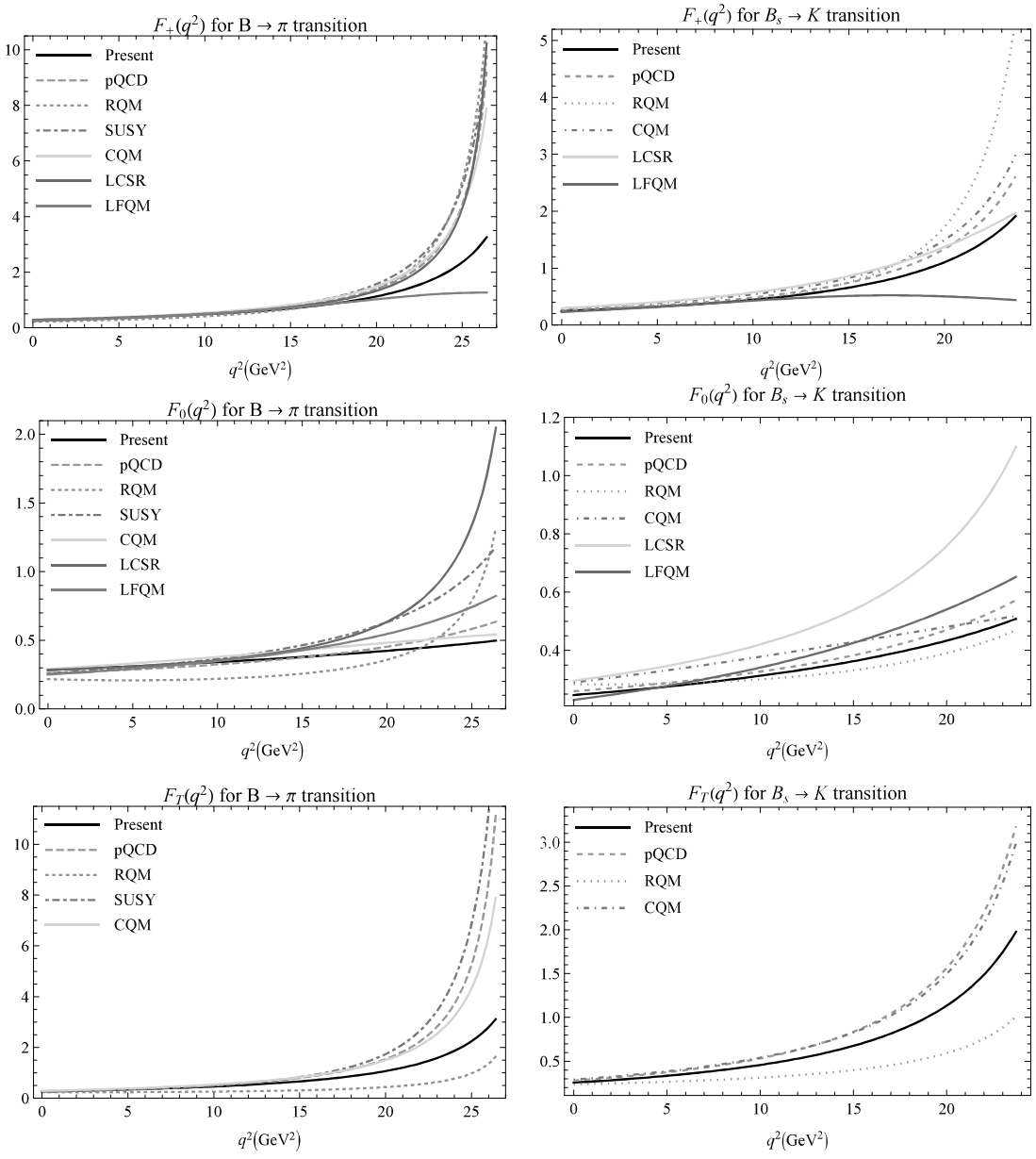

Figure 3.9: Form factors comparision for $B \to \pi$ (left) and $B_s \to K$ (right) transitions with pQCD [2], RQM [3, 4], SUSY [5], CQM [6], LCSR [7], LFQM [8].

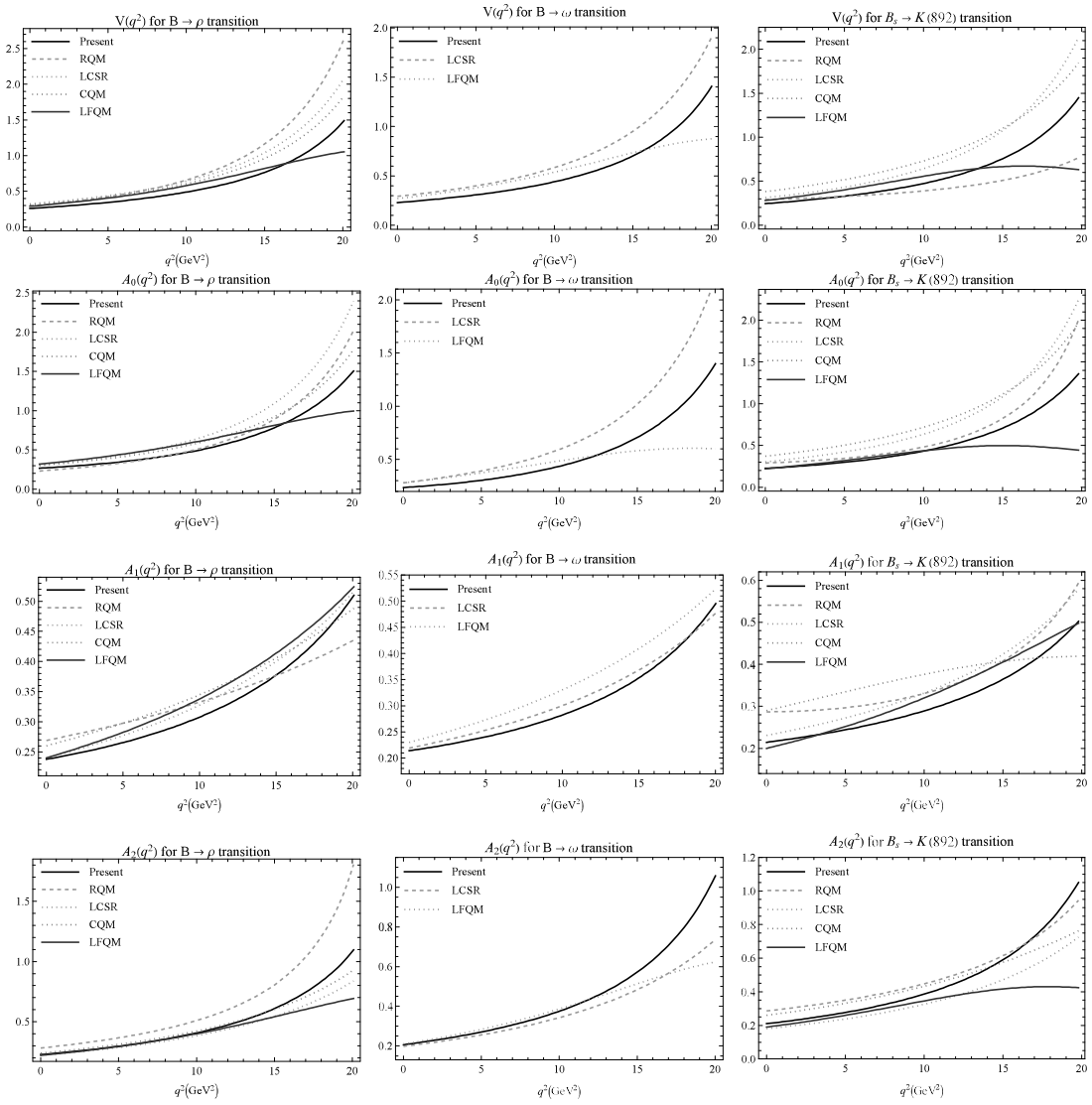

Figure 3.10: Form factors comparision for $B \to \rho$ (left), $B \to \omega$ (middle) and $B_s \to K^*(892)$ (right) transitions with RQM [3, 4], LCSR [9], CQM [6] and LFQM [8, 10].

Table 3.16: Form factors for $B \to \rho$ transitions at maximum recoil

	$V(0)$	$A_0(0)$	$A_1(0)$	$A_2(0)$	$T_{1,2}(0)$	$T_3(0)$
Present	0.259 ± 0.021	0.266 ± 0.013	0.238 ± 0.019	0.227 ± 0.018	0.233 ± 0.019	0.179 ± 0.014
LCSR [7]	0.289 ± 0.016	- - -	$0.232^{+0.013}_{-0.014}$	$0.187^{+0.011}_{-0.012}$	0.256 ± 0.015	0.175 ± 0.010
LCSR [9]	0.323	0.303	0.242	0.221	0.267	0.176
LCSR [175]	0.327 ± 0.031	0.356 ± 0.042	0.262 ± 0.026	0.297 ± 0.035	0.272 ± 0.026	0.747 ± 0.076
LCSR [49]	0.27 ± 0.14	- - -	- - -	0.19 ± 0.11	0.24 ± 0.12	- - -
pQCD [169]	$0.21^{+0.05+0.03}_{-0.04-0.02}$	$0.25^{+0.06+0.04}_{-0.05-0.03}$	$0.16^{+0.04+0.02}_{-0.03-0.02}$	$0.13^{+0.03+0.02}_{-0.03-0.01}$	$0.19^{+0.04+0.03}_{-0.04-0.02}$	$0.17^{+0.04+0.02}_{-0.03-0.02}$
SCET [167]	0.298	0.260	0.227	0.215	0.260	0.184
RQM [3]	0.295 ± 0.015	0.231 ± 0.012	0.269 ± 0.014	0.282 ± 0.014	0.290 ± 0.015	0.124 ± 0.007
CQM [6]	0.31	0.30	0.26	0.24	0.27	0.19
LFQM [10]	$0.35^{+0.01+0.06}_{-0.01-0.05}$	$0.30^{+0.01+0.05}_{-0.01-0.05}$	$0.27^{+0.01+0.05}_{-0.01-0.04}$	$0.25^{+0.01+0.04}_{-0.01-0.04}$	- - -	- - -

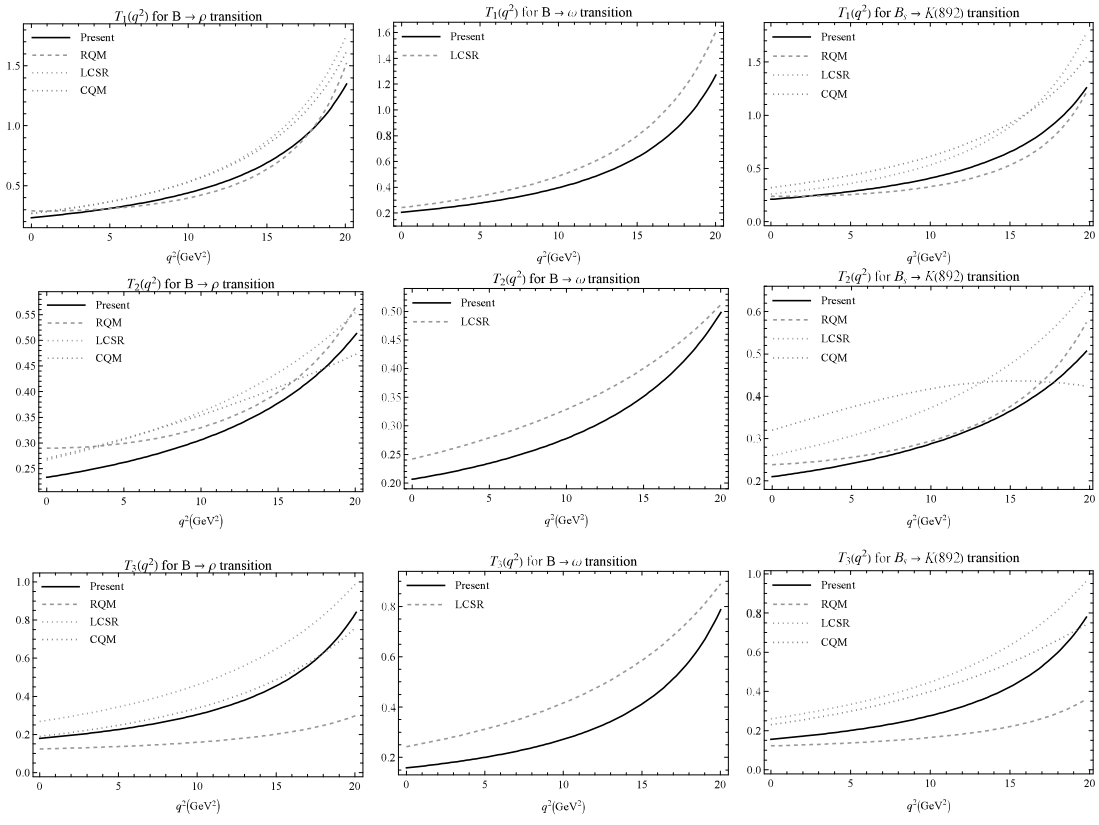

Figure 3.11: Form factors comparision for $B \to \rho$ (left), $B \to \omega$ (middle) and $B_s \to K^*(892)$ (right) transitions with RQM [3, 4], LCSR [9] and CQM [6].

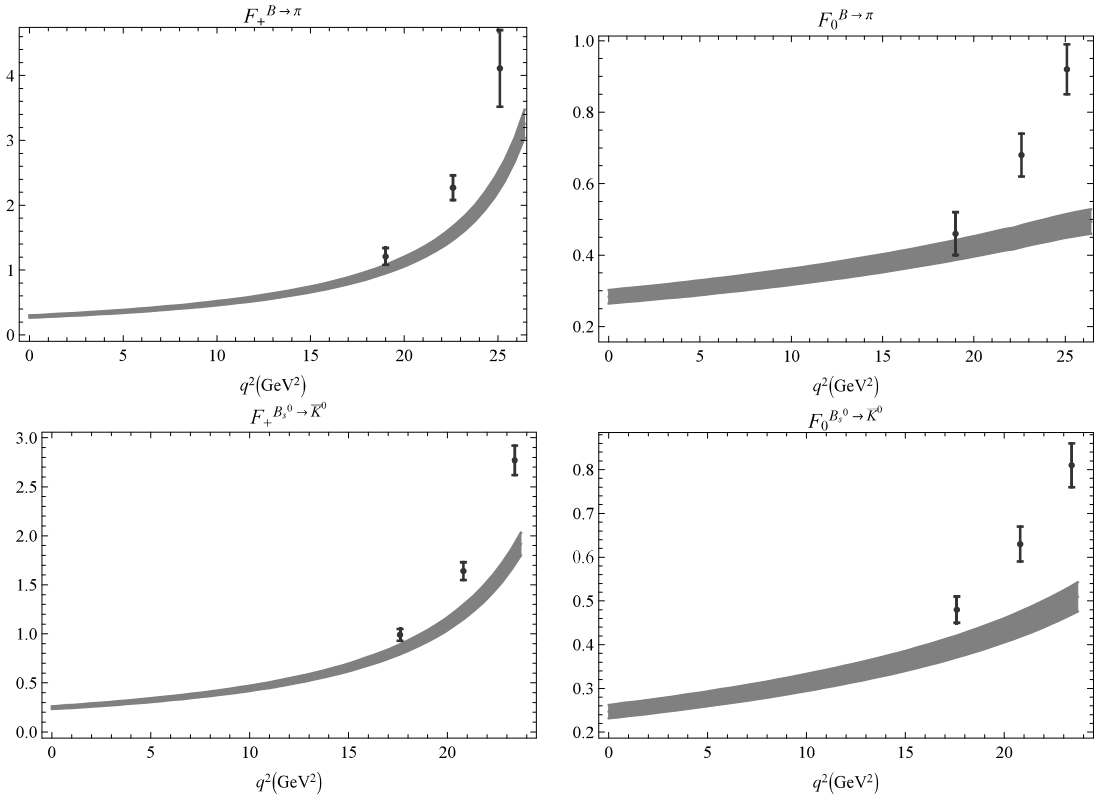

Figure 3.12: Form factor for $B \to \pi$ and $B_s \to K$ transitions (obtained in CCQM (solid broad lines) and in LQCD computations (dots with uncertainties) by RBC and UKQCD collaboration [11]).

A brief comparison of our calculated form factors with the light cone sum rules (LCSR), perturbative QCD (pQCD), supersymmetry (SUSY), relativistic quark model (RQM), soft collinear effective field theory (SCET), constituent quark models (CQM) and light front quark model (LFQM) is given in Tab. 3.15 − 3.3. Form factors are calculated at the maximum recoil value (q^2=0). Our form factors are in very good agreement with LCSR [7,47], perturbative QCD [2] and CQM [6] for $B \to \pi$ channel, where as our form factors underestimate the LCSR and CQM results but are closer with the pQCD prediction [14] for $B_s^0 \to \bar{K}^0$ channel. For pQCD Ref. [14], the form factors are calculated in perturbative QCD framework using the inputs from LQCD.

Similarly, in Tab. 3.16 and Tab. 3.17 − 3.3 we present $B \to \rho$, $B^0 \to \omega$ and $B_s^0 \to \bar{K}^*(982)^0$ transition form factors. Our results are in good agreement with the LCSR results. For $B_s^0 \to \bar{K}^*(982)^0$ channel, our form factors are also in good agreement with the pQCD approach [14].

Further, the form factors are also compared in the entire physical range of momentum transfer $0 \leq q^2 \leq q^2_{\rm max} = (m_{B_{(s)}} - m_{P/V})^2$. Fig. 3.9 - 3.11, provide the q^2 dependency of form factors in comparison with different approaches. In Fig. 3.9, the form factor comparison of $B \to \pi$ and $B_s^0 \to \bar{K}^0$ channels along with different theoretical approaches are given. It is important to note here that the form factor $F_0(q^2)$ is related

Table 3.17: Form factors for $B \to \omega$ transitions at maximum recoil

	$V(0)$	$A_0(0)$	$A_1(0)$	$A_2(0)$	$T_{1,2}(0)$	$T_3(0)$
Present	0.229 ± 0.023	0.236 ± 0.011	0.214 ± 0.017	0.206 ± 0.016	0.206 ± 0.017	0.158 ± 0.013
LCSR [7]	$0.268^{+0.014}_{-0.015}$	- - -	$0.214^{+0.013}_{-0.012}$	$0.170^{+0.010}_{-0.011}$	$0.237^{+0.013}_{-0.014}$	0.160 ± 0.009
LCSR [9]	0.293	0.281	0.219	0.198	0.242	0.155
LCSR [175]	0.304 ± 0.038	0.328 ± 0.048	0.243 ± 0.031	0.270 ± 0.040	0.251 ± 0.031	0.683 ± 0.090
pQCD [169]	$0.19^{+0.04+0.03}_{-0.04-0.02}$	$0.23^{+0.05+0.03}_{-0.04-0.02}$	$0.15^{+0.03+0.02}_{-0.03-0.01}$	$0.12^{+0.03+0.02}_{-0.02-0.01}$	$0.18^{+0.04+0.02}_{-0.04-0.02}$	$0.15^{+0.04+0.02}_{-0.03-0.02}$
SCET [167]	0.275	0.240	0.209	0.198	0.239	0.168
LFQM [8]	0.27	0.28 ± 0.01	0.23	0.21	- - -	- - -

Table 3.18: Comparison of form factors at higher q^2 values with LQCD (data from Table VI of Ref. [11]) for $B_s \to K$ and $B \to \pi$ channels

Channel	q^2	$F_+(q^2)$		$F_0(q^2)$	
	GeV^2	Present	LQCD	Present	LQCD
	17.6	0.84 ± 0.05	0.99 ± 0.06	0.40 ± 0.03	0.48 ± 0.03
$B_s \to K$	20.8	1.22 ± 0.05	1.64 ± 0.09	0.45 ± 0.03	0.63 ± 0.04
	23.4	1.81 ± 0.11	2.77 ± 0.15	0.50 ± 0.03	0.81 ± 0.05
	19.0	1.01 ± 0.07	1.21 ± 0.13	0.41 ± 0.03	0.46 ± 0.06
$B \to \pi$	22.6	1.57 ± 0.010	2.27 ± 0.19	0.45 ± 0.03	0.68 ± 0.06
	25.1	2.40 ± 0.16	4.11 ± 0.59	0.48 ± 0.03	0.92 ± 0.07

with $F_+(q^2)$ and $F_-(q^2)$ of Eq. (3.6) and (3.7) via

$$F_0(q^2) \;=\; F_+(q^2) + \frac{q^2}{m_1^2 - m_2^2} F_-(q^2) \tag{3.42}$$

Our results show a fair match with other approaches for $q^2 \leq 15$ GeV^2 for both the channels. It is also evident that our form factors $F_{+,0}(q^2)$ are in close resemblance with the form factors calculated using LFQM [8,10] and our form factors $F_{0,T}(q^2)$ are also in close resembles with CQM [6].

Fig. 3.10 − 3.11 provide the form factor comparison for the channels $B \to \rho$, $B^0 \to \omega$ and $B_s^0 \to \bar{K}^*(892)^0$ and it is seen that the form factors $V(q^2)$ and $A_{0,1,2}(q^2)$ show good agreement with other theoretical predictions for the whole q^2 range. Our results are also matching well for the form factors $T_{1,2,3}(q^2)$ with other approaches.

Our comparison of the results of form factors for the channels $B \to \pi$ and $B_s^0 \to \bar{K}^0$ with LQCD from RBC and UKQCD collaborations [11] at higher q^2 values is given in Tab. 3.18. Our result match well with LQCD predictions for intermediate q^2 range, but systematically lowers down as $q^2 \to q^2_{\rm max}$. Ref. [11] uses domain-wall light quarks and relativistic b - quarks formalism to calculate the vector and scalar form factors for $B \to \pi \ell \nu_\ell$ and $B_s \to K \ell \nu_\ell$ in LQCD at three q^2 ranges. It is interesting to note that similar trend is observed for both $B_s^0 \to \bar{K}^*(892)^0$ (Tab. 3.19) and for

$D \to (\pi, K)$ form factors in [216–218] when compared with LQCD predictions from ETM collaboration. However, the tensor form factor shows very good agreement with the ETM collaboration. In Fig. 3.12, the form factors comparison for the channels $B \to \pi$ and $B_s^0 \to \bar{K}^0$ with LQCD predictions [11] are given. We also present the spread of our form factors in the whole q^2 range corresponding to the uncertainties in the fitting parameters. Similar spread can also be obtained for the vector meson form factors.

All model dependent and independent parameters along with the form factors are taken into account to compute the branching fractions using Eq. (3.25). Our results

Table 3.19: Comparison of form factors at higher q^2 (in GeV^2) values with LQCD [15] for $B_s \to K^*(892)$ channel

$F(q^2)$		$q^2 = 12$	$q^2 = 16$	$q^2 = q^2_{\rm max}$
$V(q^2)$	Present	0.56 ± 0.04	0.85 ± 0.06	1.50 ± 0.10
	LQCD	0.56 (9)	1.02 (8)	1.99 (13)
$A_0(q^2)$	Present	0.52 ± 0.06	0.79 ± 0.09	1.41 ± 0.13
	LQCD	0.84 (9)	1.33 (8)	2.38 (16)
$A_1(q^2)$	Present	0.31 ± 0.02	0.38 ± 0.03	0.51 ± 0.03
	LQCD	0.37 (3)	0.45 (3)	0.58 (3)
$A_2(q^2)$	Present	0.45 ± 0.03	0.65 ± 0.04	1.08 ± 0.07
	LQCD	0.46 (3)	0.60 (5)	0.85 (12)
$T_1(q^2)$	Present	0.48 ± 0.03	0.73 ± 0.05	1.30 ± 0.09
	LQCD	0.61 (4)	0.90 (6)	1.48 (10)
$T_2(q^2)$	Present	0.31 ± 0.02	0.39 ± 0.03	0.52 ± 0.04
	LQCD	0.39 (3)	0.47 (3)	0.60 (3)
$T_3(q^2)$	Present	0.32 ± 0.04	0.47 ± 0.05	0.80 ± 0.06
	LQCD	0.43 (4)	0.67 (5)	1.10 (7)

Table 3.20: Partial branching fractions for $B^+ \to \pi^+\mu^+\mu^-$ in Unit of 10^{-9}

q^2 bin	Nonresonant	Resonant	LQCD [215]	LCSR [50]
$[0.05, 2.0]$	2.37 ± 0.33	3.62 ± 0.43	- - -	$2.49^{+0.30}_{-0.20}$
$[0.1, 2.0]$	2.32 ± 0.33	3.58 ± 0.42	1.81	- - -
$[2.0, 4.0]$	2.50 ± 0.35	2.81 ± 0.40	1.92	$1.56^{+0.09}_{-0.08}$
$[4.0, 6.0]$	2.54 ± 0.35	2.88 ± 0.41	1.91	$1.39^{+0.16}_{-0.11}$
$[6.0, 8.0]$	2.65 ± 0.37	3.20 ± 0.45	1.89	$1.28^{+0.30}_{-0.23}$
$[15, 17]$	1.48 ± 0.21	1.41 ± 0.19	1.69	- - -
$[17, 19]$	1.20 ± 0.17	1.10 ± 0.17	- - -	- - -
$[19, 22]$	1.23 ± 0.17	1.12 ± 0.17	1.84	- - -
$[22, 25]$	0.52 ± 0.07	0.48 ± 0.07	1.07	- - -
$[1.0, 6.0]$	6.28 ± 0.89	7.66 ± 1.06	4.78	$1.68^{+0.16}_{-0.12}$
$[15, 22]$	3.90 ± 0.54	3.62 ± 0.50	5.05	- - -
$[4m_\ell^2, q^2_{max}]$	21.73 ± 3.04	- - -	20.4	- - -

with and without resonant counterparts from the charmed (J/ψ and $\psi(2S)$) and charmless (ρ, ω and ϕ) vector meson resonances are also calculated. We avoid the q^2 range close to the $q^2 = m^2_{J/\psi}$ and $q^2 = m^2_{\psi(2S)}$ for the computation of resonant branching fractions, as experimental analysis also excludes these resonance regions. The experimentally vetoed regions corresponding to J/ψ and $\psi(2S)$ are $8.0 < q^2 < 11.0$ GeV^2 and $12.5 < q^2 < 15.0$ GeV^2, respectively. It is important to note here that when we consider the resonances for branching fraction computations, the results are enhanced by an order or two. Similar observations have also been reported in a review [194]. We also exclude the experimentally vetoed regions, in order to compare our results with experimental data. Different treatments are available in the literature to handle these resonance regions. For example, in Ref. [219], the resonance regions are smoothed-out by including the next-to-leading order correction in $C_9^{\rm eff}$ using the auxiliary functions $F_{1,2}^{(7,9)}(q^2)$ from the ref. [220]. In Tab. 3.20, our results of branching fractions for $B^+ \to \pi^+\mu^+\mu^-$ in narrow q^2 bins are compared with LQCD and LCSR results and our results are notably on higher side. It should also be noted that the results from most of the theory attempts are systematically higher than LHCb data in the narrow q^2 bins [198]. Our results of rare decays of B and B^0 mesons are compared with theoretical approaches viz. LCSR [7] and RQM [4] in Tab. 3.13. Note that the results presented in Refs. [4, 7] correspond to the non-resonant contributions. LHCb collaboration has provided the branching fractions for $B^+ \to \pi^+\mu^+\mu^-$ and our resonant result is lower than LHCb data. For the other channels, only the upper bounds are provided in PDG. Further, our results match with the upper limit of Belle [43] and *BABAR* [221, 222] collaborations results for $B^0 \to \pi^0\ell^+\ell^-$ with $\ell = e$ and μ channel. The experimental data is not reported for $B^+ \to \rho^+\ell^+\ell^-$ and $B^0 \to$

Table 3.21: Ratios of the Branching fractions

Ratio	Unit	Present	Data
$\frac{\mathcal{B}(B^+\to\pi^+\mu^+\mu^-)}{\mathcal{B}(B^+\to K^+\mu^+\mu^-)}$	10^{-2}	3.02 ± 0.42	$5.3 \pm 1.4 \pm 0.1$ [42]
$\frac{\mathcal{B}(B^+\to\rho^+\mu^+\mu^-)}{\mathcal{B}(B^+\to K^*(892)^+\mu^+\mu^-)}$	10^{-2}	3.19 ± 1.14	- - -
$\frac{\mathcal{B}(B_s^0\to\bar{K}^*(892)^0\mu^+\mu^-)}{\mathcal{B}(B^0\to K^*(892)^0\mu^+\mu^-)}$	10^{-2}	2.61 ± 0.74	$3.3 \pm 1.1 \pm 0.3 \pm 0.2$ [213]

$(\rho^0, \omega)\ell^+\ell^-$ channels. For the $B^{+(0)} \to (\rho^{+(0)}, \omega)\nu\bar{\nu}$ channels, our results are well within the upper limit of PDG data. For the channel $B_s^0 \to \bar{K}^*(892)^0\mu^+\mu^-$ (Tab. 3.14), our results are within the range predicted in the LHCb data and experimental results are unavailable for the other rare B_s decay. Muon channel to electron channel ratio for $B^+ \to \pi^+$ and $B^0 \to \pi^0$ tends to be 1, whereas for the $B^{+(0)} \to (\rho^{+(0)}, \omega)$, our calculated ratio turns out to be 0.85. However, if the uncertainties in form factors are transported to corresponding branching fractions, the ratio approaches unity. The non-resonant branching fractions corresponding to $B^+ \to (\pi^+, \rho^+)\ell^+\ell^-$ for $\ell = e,\ \mu$ are in good agreement with the LCSR and μ channel of RQM results, whereas for B_s^0 channels, the calculated results are systematically lower than both LCSR and RQM results. Our results agrees well with the uncertainties of LCSR for the $B^0 \to (\pi^0, \rho^0, \omega)\ell^+\ell^-$ and $B^+ \to \rho^+\tau^+\tau^-$ channels. Further the radiative decays have also been computed and it is evident that the calculated results on $\mathcal{B}(B^+ \to \rho^+\gamma)$ matches well with the results reported by LHCb. Our results on $\mathcal{B}(B_s^0 \to \bar{K}^*(892)^0\gamma)$ are also within the uncertainty window of LHCb data but disagree with the RQM and LCSR results.

Rare decays corresponding the $b \to s$ transitions was also studied in great details employing CCQM in [210, 223] by Dubničkа *et al*. In these articles the branching fractions for $B \to K^{(*)}\ell^+\ell^-$ and $B_s \to \phi\ell^+\ell^-$ for $\ell = e, \mu, \tau$ is computed. Taking the inputs from these papers, we compute the ratios of $b \to s$ to $b \to d$ rare decays and they are tabulated in Tab. 3.21. It is important to highlight that the calculated ratios are within the range predicted by the LHCb data except for the ratio $\mathcal{B}(B^+ \to \pi^+\mu^+\mu^-)/\mathcal{B}(B^+ \to K^+\mu^+\mu^-)$ where our result underestimate the LHCb data. We have also calculated few physical observables like forward-backward asymmetry, longitudinal and transverse polarization. This work was published in [224]. The detailed calculation technique and results for other observables will be discussed in the next chapter.